

# Root development is maintained by specific bacteria-bacteria interactions within a complex microbiome

**Authors:** Omri M. Finkel<sup>1,2†</sup>, Isai Salas-González<sup>1,2,3†</sup>, Gabriel Castrillo<sup>1,2‡</sup>, Theresa F. Law<sup>1,2</sup>, Jonathan M. Conway<sup>1,2</sup>, Paulo José Pereira Lima Teixeira<sup>1,2¤</sup>, Corbin D. Jones<sup>1,3,4,5,6,7</sup>, Jeffery L. Dangl<sup>1,2,3,6,7,8\*</sup>

**Affiliations:**

<sup>1</sup>Department of Biology, University of North Carolina at Chapel Hill, Chapel Hill, North Carolina, United States of America.

<sup>2</sup>Howard Hughes Medical Institute, University of North Carolina at Chapel Hill, Chapel Hill, North Carolina, United States of America.

<sup>3</sup>Curriculum in Bioinformatics and Computational Biology, University of North Carolina at Chapel Hill, Chapel Hill, North Carolina, United States of America.

<sup>4</sup>Department of Genetics, University of North Carolina at Chapel Hill, Chapel Hill, North Carolina, United States of America.

<sup>5</sup>Lineberger Comprehensive Cancer Center, University of North Carolina at Chapel Hill, Chapel Hill, North Carolina, United States of America.

<sup>6</sup>Carolina Center for Genome Sciences, University of North Carolina at Chapel Hill, Chapel Hill, North Carolina, United States of America.

<sup>7</sup>Curriculum in Genetics and Molecular Biology, University of North Carolina at Chapel Hill, Chapel Hill, North Carolina, United States of America.

<sup>8</sup>Department of Microbiology and Immunology, University of North Carolina at Chapel Hill, Chapel Hill, North Carolina, United States of America.

\*Correspondence to: dangl@email.unc.edu

†These authors contributed equally to this work.

‡Current address: Future Food Beacon of Excellence and the School of Biosciences, University of Nottingham, Sutton Bonington, United Kingdom

¤Current address: Department of Biology, “Luiz de Queiroz” College of Agriculture (ESALQ), University of São Paulo (USP), Piracicaba, São Paulo, Brazil

1 **Abstract**

2 Plants grow within a complex web of species interacting with each other and with the plant via a  
3 wide repertoire of chemical signals. To model plant-microbe-microbe-environment interactions,  
4 we inoculated seedlings with a defined 185-member bacterial synthetic community (SynCom),  
5 and manipulated the abiotic environment to enable classification of the SynCom to modules of  
6 co-occurring strains. We deconstructed the SynCom based on these modules, identifying a single  
7 bacterial genus, *Variovorax*, which reverts phenotypic effects on root development induced by a  
8 wide diversity of bacterial strains and by the entire 185-member community. *Variovorax* use  
9 mechanisms related to auxin and ethylene manipulation to balance this ecologically realistic root  
10 community's effects on root development. We demonstrate metabolic signal interference within a  
11 complex model community, defining *Variovorax* as determinants of bacteria-plant communication  
12 networks.

13

14 **Introduction**

15 Plant phenotypes, and ultimately fitness, are influenced by the microbes living in close association  
16 with them (1–4). This plant microbiota assembles based on plant-derived cues (5) resulting in  
17 myriad plant-microbe interactions. Beneficial and detrimental microbial effects on plants can be  
18 direct, via production of chemical signals (6, 7) or modulation of nutrient availability (1, 4, 8); or  
19 they can be an indirect consequence of microbe-microbe interactions (3). A potentially significant  
20 class of microbe-microbe interactions is metabolic signal interference (7, 9): rather than direct  
21 antagonism, microbes interfere with the delivery of chemical signals produced by other microbes,  
22 altering plant-microbe signaling (10–12).

23

24 Here, we apply a plant microbiota synthetic community (SynCom) to axenic plants, to ask how  
25 microbe-microbe interactions shape plant phenotypes. We used plant colonization patterns  
26 across 16 abiotic conditions to guide stepwise deconstruction of the SynCom, leading to the  
27 identification of a single bacterial genus that is required for maintaining the root's intrinsically  
28 controlled developmental program by tuning its chemical landscape.

29

30 **Results**

31 We established a controlled plant-microbiota microcosm representing the native bacterial  
32 microbiota on agar plates. We inoculated 7-day-old seedlings with a defined 185-member  
33 bacterial SynCom (fig. S1 and data S1) composed of genome-sequenced isolates obtained from

34 Arabidopsis roots (Material and Methods 1). To test the robustness of microbiota assembly to the  
35 abiotic environment, we exposed each microcosm to one of 16 different abiotic contexts by  
36 manipulating four variables (salinity, temperature, phosphate concentration and pH). We  
37 measured SynCom composition in root, shoot and agar fractions 12 days post-inoculation using  
38 16S rRNA amplicon sequencing. Across all abiotic variables, fraction (agar, root, shoot; fig. S2)  
39 explained most (40%) of the variance. Abiotic conditions significantly affected both alpha- (fig. S3)  
40 and beta-diversity (Fig. 1A). Our SynCom therefore exhibits deterministic niche sorting within the  
41 plant across a range of abiotic conditions.

42  
43 We calculated pairwise correlations in relative abundance across all samples, and identified four  
44 well-defined modules of co-occurring strains (A, B, C and D; Fig. 1B and data S2). These modules  
45 formed distinct phylogenetically-structured guilds in association with the plant: module A  
46 contained mainly Gammaproteobacteria and was predominantly more abundant in the agar than  
47 in the seedling; module B contained mainly low-abundance Firmicutes, with no significant  
48 seedling enrichment trend; modules C and D were composed mainly of Alphaproteobacteria and  
49 Actinobacteria, respectively, and showed seedling-enrichment across all abiotic conditions  
50 (Figure 1A and data S2). Both Alphaproteobacteria (module C) and Actinobacteria (module D)  
51 are consistently plant-enriched across plant species (13), suggesting that they contain plant-  
52 association traits that are deeply rooted in their evolutionary histories.

53  
54 We next asked whether the different modules of co-occurring strains play different roles in  
55 determining plant phenotypes (Materials and Methods 2). We inoculated seedlings with SynComs  
56 composed of modules A, B, C and D singly, or with all six possible pairwise module combinations  
57 (Fig. 2A), and imaged the seedlings 12 days post-inoculation. We observed strong primary root  
58 growth arrest in seedlings inoculated with plant-enriched modules C or D (Fig. 2A). This root  
59 growth inhibition (RGI) did not occur in seedlings inoculated with modules A or B, which do not  
60 contain plant-enriched strains (Fig. 2A, 2C and data S3). To test whether plant-enrichment and  
61 RGI are correlated traits, we inoculated seedlings in mono-association with each of the 185  
62 SynCom members (Materials and Methods 3). Surprisingly, we observed that RGI-inducing  
63 strains were found in all four modules (Fig. 2B, fig. S4-S5 and data S4). Thus, in line with (4),  
64 plant-enrichment within a bacterial community does not predict phenotypic effects on seedlings  
65 in mono-association.

66

67 The mono-association assay confirmed that RGI is a prevalent trait across the plant bacterial  
68 microbiota. Thirty-four taxonomically diverse strains, derived from all four modules, induced RGI.  
69 However, neither the full SynCom nor derived SynComs of modules A or B exhibited RGI (Fig.  
70 2A), suggesting that microbe-microbe interactions are responsible for RGI attenuation within  
71 these SynComs. Furthermore, in seedlings inoculated with module pairs, we observed an  
72 epistatic interaction: in the presence of module A, RGI caused by modules C and D was reverted  
73 (Fig. 2A). Thus, through deconstructing the SynCom into four modules, we found that bacterial  
74 effects on root development are governed by multiple levels of microbe-microbe interactions,  
75 exemplified by at least four instances: within modules A and B and between module A and  
76 modules C and D. Since three of these interactions involve module A, we predicted that this  
77 module contains strains that strongly attenuate RGI, preserving stereotypic root development.

78

79 To identify strains within module A responsible for intra- and inter-module RGI attenuation, we  
80 reduced our system to a tripartite plant-microbe-microbe system (Materials and Methods 4). We  
81 individually screened the 18 non-RGI strains from module A for their ability to attenuate RGI  
82 caused by representative strains from all four modules. We found that all strains from a single  
83 genus, *Variovorax* (Family Comamonadaceae) suppressed RGI caused by representative RGI-  
84 inducing strains from module C (*Agrobacterium* MF224) and module D (*Arthrobacter* CL28; Fig.  
85 2D, fig. S6 and data S5). The strains from modules A (*Pseudomonas* MF48) and B (*Bacillus*  
86 MF107), were not suppressed by *Variovorax*, but rather by two closely related *Burkholderia*  
87 strains (CL11, MF384). A similar pattern was observed when we screened three selected RGI-  
88 suppressor *Variovorax* strains (CL14, MF160) and *Burkholderia* CL11, against a diverse set of  
89 RGI-inducers. *Variovorax* attenuated 13 of the 18 RGI-inducers tested (Fig. 2E-F, fig. S6 and data  
90 S6).

91

92 We further tested if our RGI-suppressor strains maintain their capacity to attenuate RGI in the  
93 context of the full 185-member community (Materials and Methods 5). We compared the root  
94 phenotype of seedlings exposed to either the full SynCom or to the same community dropping-  
95 out all ten *Variovorax* strains and/or all six *Burkholderia* strains (drop-out system, Fig. 3A-C). We  
96 found that *Variovorax* are necessary and sufficient to revert RGI within the full community (Fig.  
97 3B-C and data S7). This result was robust across a range of biotic and abiotic contexts (Fig. 3D-  
98 E, fig. S7-S8 and data S7; Materials and Methods 6-7).

99

100 To ascertain the phylogenetic breadth of the *Variovorax* ability to attenuate RGI, we tested  
101 additional *Variovorax* strains from across the genus' phylogeny (fig. S9A and data S1; Materials  
102 and Methods 8). All tested *Variovorax* reverted RGI induced by *Arthrobacter* CL28 (Materials and  
103 Methods 9). A strain from the nearest plant-associated outgroup to this genus, *Acidovorax*  
104 Root219, did not revert RGI (fig. S9A-B and data S8). *Variovorax*-mediated RGI attenuation  
105 extended to tomato seedlings, where *Variovorax* CL14 reverted *Arthrobacter* CL28-mediated RGI  
106 (fig. S10, data S9, Materials and Methods 10). Thus, a single bacterial genus, *Variovorax*,  
107 interacts with a wide diversity of bacteria to enforce stereotypic root development within complex  
108 communities, independent of biotic or abiotic contexts, and this ability is general to this genus.  
109

110 We tested whether *Variovorax* attenuate RGI by inhibiting growth of RGI-inducing strains  
111 (Materials and Methods 11). We counted colony forming units of the RGI inducer *Arthrobacter*  
112 CL28 from roots in the presence or absence of *Variovorax* CL14 and found that CL28 abundance  
113 increased in the presence of *Variovorax* CL14 (fig. S11, data S10). To test whether *Variovorax*  
114 modulates bacterial abundances in the whole community, we compared the bacterial relative  
115 abundance profiles in seedlings colonized with the full SynCom to that colonized with the  
116 *Variovorax* drop-out community (Materials and Methods 6d). We found no changes in the  
117 abundances of RGI-inducing strains in response to the *Variovorax* drop-out (Fig. 3F). In fact,  
118 *Variovorax* account for <1% of the community on our roots (Fig. 3G), and in natural soils (fig.  
119 S12). Notably, while rare, *Variovorax* are root-enriched in two natural soils tested (fig. S12). These  
120 results rule out the possibility that *Variovorax* enforce root developmental patterns by  
121 antagonizing or outcompeting RGI-inducers. We hypothesized that RGI attenuation by *Variovorax*  
122 is likely mediated by signal interference.  
123

124 To study the mechanisms underlying RGI and RGI attenuation, we analyzed the transcriptomes  
125 of seedlings colonized for 12 days with the RGI-inducer *Arthrobacter* CL28 and the RGI-attenuator  
126 *Variovorax* CL14, either in mono-association with the seedling or in a tripartite combination (Fig.  
127 2F; Materials and Methods 12). We also performed RNA-Seq on seedlings colonized with the full  
128 SynCom (no RGI) or the *Variovorax* drop-out SynCom (RGI; Fig. 3A). Eighteen genes were  
129 significantly induced only under RGI conditions across both experiments (Fig. 4A-B and data  
130 S11). Seventeen of these are co-expressed genes related to the root apex (14) (Fig 4B and fig.  
131 S13). The remaining gene is Indole-3-acetic acid-amido synthetase GH3.2, which conjugates  
132 excess amounts of the plant hormone auxin and is a robust marker for late auxin responses (15,  
133 16) (Fig. 4C). Production of auxins is a well-documented mechanism by which bacteria modulate

134 plant root development (10). Indeed, the top 12 auxin-responsive genes from an RNA-Seq study  
135 examining acute auxin response in *Arabidopsis* (15) exhibited an average transcript increase in  
136 seedlings exposed to our RGI-inducing conditions (Fig. 4C and data S12).

137  
138 Next, we asked whether RGI-attenuation by *Variovorax* is directly and exclusively related to auxin  
139 signaling (Materials and Methods 13). Besides auxin, other small molecules cause RGI. These  
140 include the plant hormones ethylene (17) and cytokinin (18); and microbial-associated molecular  
141 patterns (MAMPs) including the flagellin-derived peptide flg22 (19). We tested the ability of  
142 diverse *Variovorax* strains and of the *Burkholderia* strain CL11 to revert RGI induced by auxins  
143 (Indole-3-acetic acid [IAA] and the auxin analogue 2,4-Dichlorophenoxyacetic acid [2,4-D]),  
144 ethylene (the ethylene precursor 1-Aminocyclopropane-1-carboxylic acid [ACC]), cytokinins  
145 (Zeatin, 6-Benzylaminopurine) and flg22 peptide (fig. 4D). All tested *Variovorax* suppress RGI  
146 induced by IAA or ACC (Figure 4D and data S13), with the exception of *Variovorax* YR216 which  
147 did not suppress ACC-induced RGI and does not contain an ACC deaminase gene (fig. S9A), a  
148 plant growth-promoting feature associated with this genus (17). *Burkholderia* CL11 was only able  
149 to partially revert ACC-induced RGI. None of the *Variovorax* attenuated RGI induced by 2,4-D, by  
150 flg22 or by cytokinins, indicating that *Variovorax* revert RGI induction by interfering with auxin  
151 and/or ethylene signaling. Furthermore, this function is mediated by recognition of auxin by the  
152 bacteria and not by the plant auxin response *per se* since RGI induced by 2,4-D is not reverted.  
153 Indeed, we found that *Variovorax* CL14 degrades IAA *in-vitro* (fig. S14; Materials and Methods  
154 14) and quenches fluorescence of the *Arabidopsis* auxin reporter line *DR5::GFP* caused by the  
155 RGI inducer *Arthrobacter* CL28 (Fig. 4E, fig. S15 and data S14; Materials and Methods 15).

156  
157 We used the auxin-insensitive *axr2-1* mutant (20), combined with a competitive inhibitor of  
158 ethylene receptors, 1-Methylcyclopropene (1-MCP) (21), to examine the roles of plant auxin and  
159 ethylene perception in bacterially-induced RGI (Materials and Methods 16). We inoculated wild  
160 type seedlings and the *axr2-1* mutants, treated or not with 1-MCP, with the RGI-inducing  
161 *Arthrobacter* CL28 or the *Variovorax* drop-out SynCom. We observed in both cases that bacterial  
162 RGI is reduced in *axr2-1* and 1-MCP-treated wild type seedlings, and is further reduced in doubly-  
163 insensitive 1-MCP-treated *axr2-1* seedlings, demonstrating a synergistic effect of auxin and  
164 ethylene (Fig. 4F and data S15) on bacterial RGI. Thus, a complex SynCom can induce severe  
165 morphological changes in root phenotypes via both auxin- and ethylene-dependent pathways,  
166 and both are reverted when *Variovorax* are present. We conclude that seedlings growing in a  
167 realistically diverse bacterial microbiota depend on specific taxa for maintaining a controlled

168 developmental program by tuning the root's response to its microbially-encoded chemical  
169 landscape.

170

## 171 **Discussion**

172 Microbes communicate with the plant and each other by secreting a wide repertoire of secondary  
173 metabolites, which have profound effects on plant physiology and development (10, 19). Equally  
174 important are the interactions between these signals, as in the case of quorum quenching (12) or  
175 degradation of MAMPs (22). The degradation of bacterially-produced auxin is prevalent in the  
176 rhizosphere, including among *Variovorax* (10, 11, 23), but its consequences for the plant have  
177 not been demonstrated in a community context. Intriguingly, sequenced *Variovorax* genomes do  
178 not contain any canonical auxin degradation operons (Materials and Methods 18) (23), suggesting  
179 a novel mechanism. This work demonstrates metabolic signal interference from within a complex  
180 model community and stages *Variovorax* as key players in bacteria-plant communication  
181 networks, demonstrating an ability to block bacterial effects on root development across a wide  
182 range of biotic and abiotic contexts.

183

184 Signaling molecules and other secondary metabolites are products of evolution towards  
185 increasing complexity that allows microbes to survive competition for primary metabolites. Our  
186 results illuminate the importance of an additional trophic layer of microbes that utilize these  
187 secondary metabolites for their own benefit, while providing the unselected exaptation (24) of  
188 metabolic signal interference between the bacterial microbiota and the plant host. This potential  
189 exaptation, and the consequent homeostasis of plant hormone signals that emerges from it,  
190 allows the plant to maintain its root developmental program within a chemically rich matrix.  
191 Moreover, our data suggest that *Variovorax* accomplish this function while not disrupting the  
192 colonization of other taxa, some of which likely provide the host additional ecosystem services.  
193 As we proceed to design and develop plant probiotics, we need to consider the maintenance of  
194 intra-and inter-taxa microbial homeostasis as potential contributors to satisfactory invasion and  
195 persistence of probiotic strains into standing heterogeneous microbial communities.

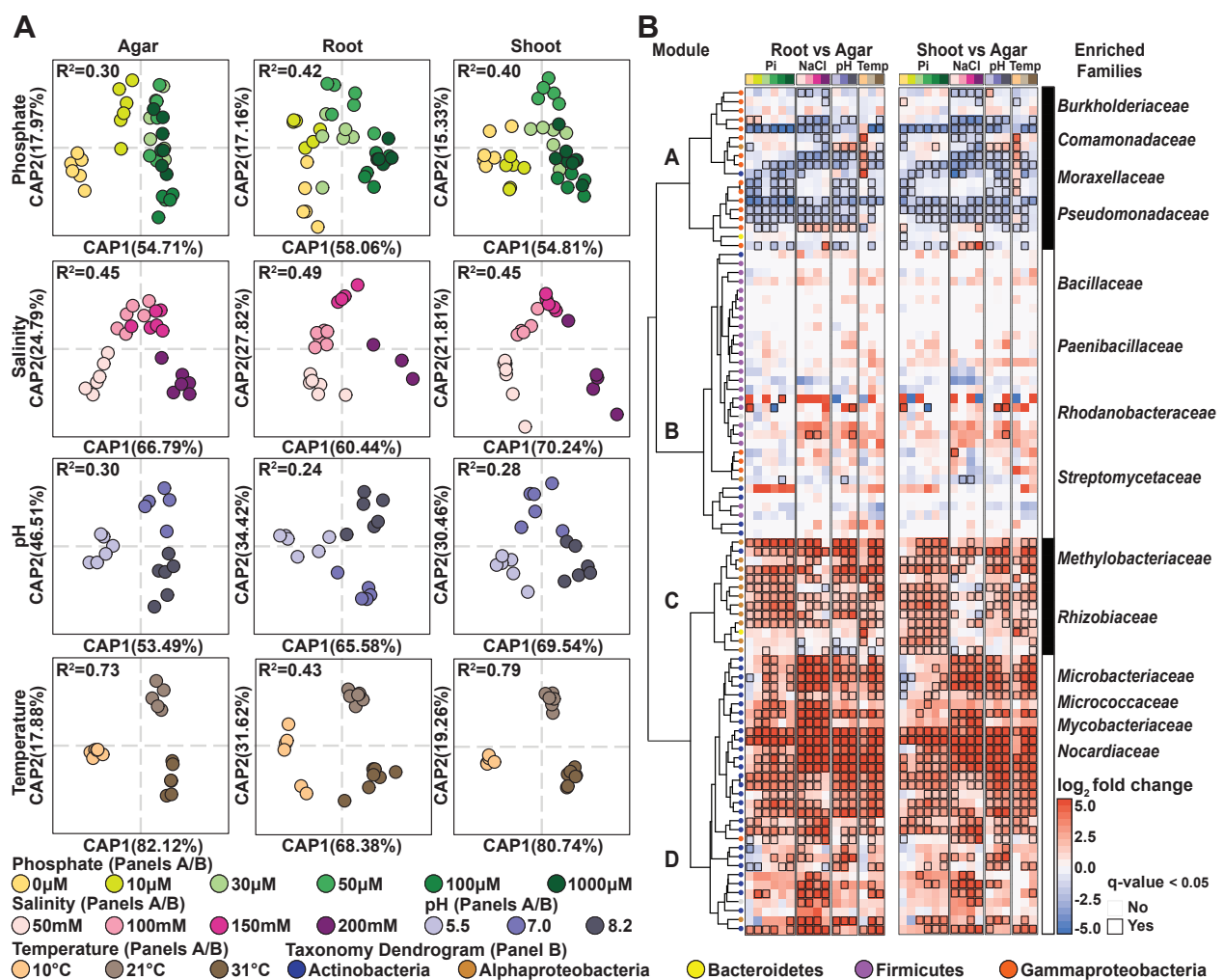


**Fig. 1. Reproducible effects of abiotic conditions on the synthetic community assembly.**

**(A)** Canonical analysis of principal coordinates (CAP) scatterplots showing the influence of each of the four abiotic gradients (phosphate, salinity, pH, temperature) within agar, root and shoot fractions. PERMANOVA  $R^2$  values are shown within each plot. **(B)** Fraction enrichment patterns of the SynCom across abiotic gradients. Each row represents a USeq. Letters on the dendrogram represent the four modules of co-occurring strains (A, B, C, D). Dendrogram tips are colored by taxonomy. The heatmaps are colored by log<sub>2</sub> fold changes derived from a fitted GLM. Positive fold changes (red gradient) represent enrichments in plant tissue (root or shoot) compared with agar, negative fold changes (blue gradient) represent depletion in plant tissue compared with agar. Comparisons with  $q$ -value  $< 0.05$  are contoured in black. Family bar highlights enriched families within each module.

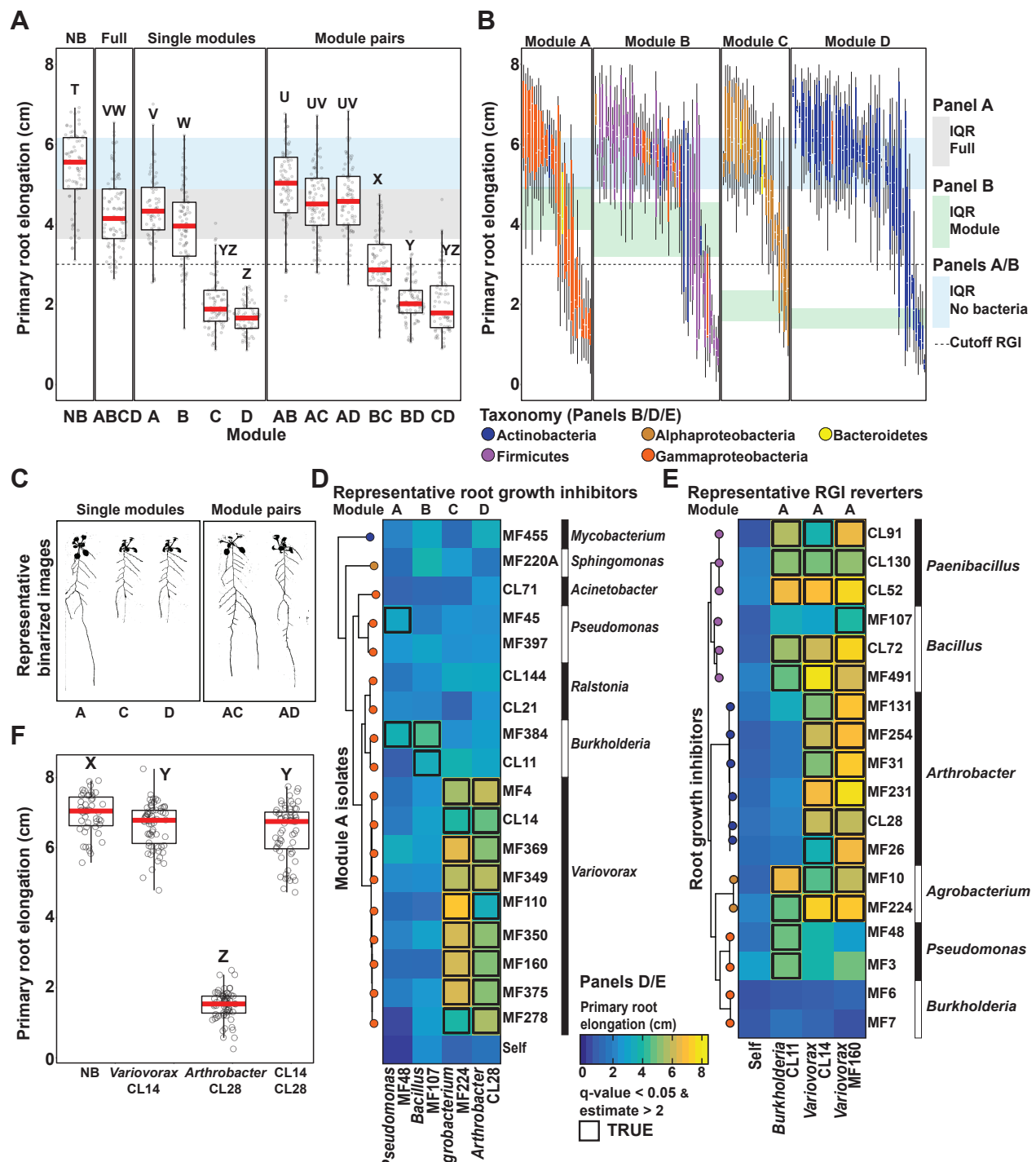


**Fig. 2. Arabidopsis root length is governed by multiple bacteria-bacteria interactions within a community.**

**(A)** Primary root elongation of seedlings grown with no bacteria (NB), with the full 185-member SynCom (Full) or with its subsets: Modules A, B, C and D alone (single modules), as well as all six possible pairwise combination of modules (module pairs). Differences between treatments are denoted using the compact letter display. **(B)** Primary root elongation of seedlings inoculated with single bacterial isolates. Isolates are colored by taxonomy and grouped by module membership. The strips across the panels correspond to the interquartile range (IQR) as noted at far right. The dotted line represents the cutoff used to classify isolates as root growth inhibiting (cutoff RGI). **(C)** Binarized image of representative seedlings inoculated with modules A, C and D, and with module combinations AC and AD. **(D, E)** Heatmaps colored by average primary root elongation of seedlings inoculated with different pairs of bacterial isolates: **(D)** with four representative RGI-inducing strains from each module (columns) alone (Self) or in combination with isolates from module A (rows), **(E)** with eighteen RGI-inducing strains (rows) alone (Self) or in combination with *Burkholderia* CL11, *Variovorax* CL14 or *Variovorax* MF160 (columns). Statistically significant RGI reversions are contoured in black. **(F)** Primary root elongation of uninoculated seedlings (NB) or seedlings inoculated with *Arthrobacter* CL28 and *Variovorax* CL14 isolates individually or jointly. Letters indicate post-hoc significance.

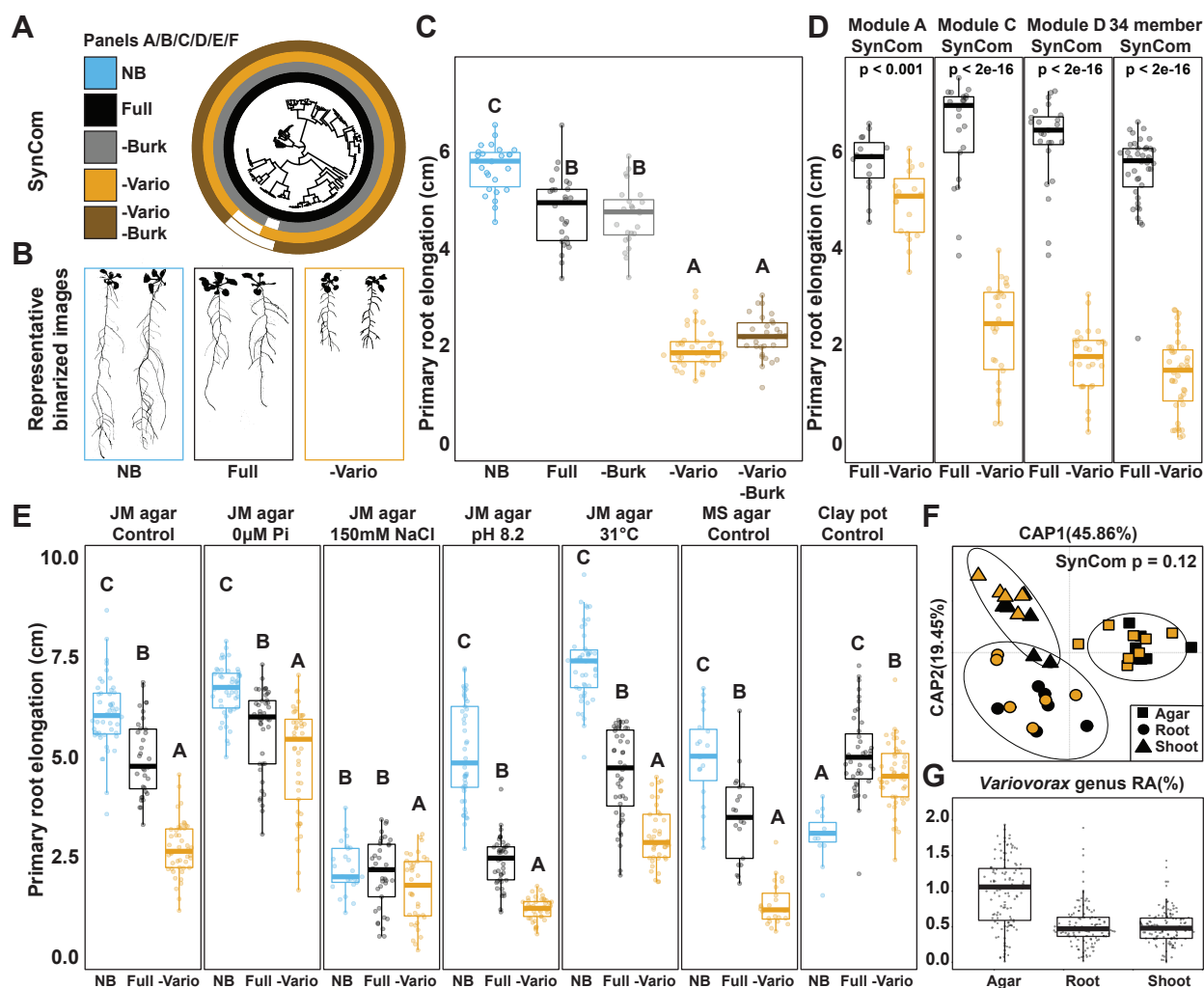


**Fig. 3** *Variovorax* are necessary and sufficient to maintain stereotypic root development.

**(A)** Phylogenetic tree of 185 bacterial isolates. Concentric rings represent isolate composition of each SynCom treatment (-Burk: *Burkholderia* drop-out, -Vario: *Variovorax* drop-out). **(B)** Binarized image of representative uninoculated seedlings (NB), or seedlings with the full SynCom (Full) or the *Variovorax* drop-out SynCom (-Vario) treatments. **(C)** Primary root elongation of uninoculated seedlings (NB) or seedlings with the different SynCom treatments. **(D)** Primary root elongation of seedlings inoculated independently with four compositionally different SynComs (Module A, C, D and 34-member) with (Full) or without (Vario) 10 *Variovorax* isolates. FDR-corrected p-values are shown within each plot. **(E)** Primary root elongation of uninoculated seedlings (NB), or seedlings with the Full SynCom or with the *Variovorax* drop-out SynCom (-Vario) across different abiotic conditions: unamended medium (JM agar control), phosphate starvation (JM agar 0  $\mu$ M Pi), salt stress (JM agar 150 mM NaCl), high pH (JM agar pH 8.2) and high temperature (JM agar 31  $^{\circ}$  C) and media: Johnson Medium (JM agar control), Murashige and Skoog (MS agar control) and calcined clay (Clay pot control). Letters indicate statistical significance. **(F)** Canonical analysis of principal coordinates scatterplots comparing community full vs *Variovorax* drop-out SynComs across all fractions (agar, root, shoot). PERMANOVA p-value is shown. **(G)** Relative abundance (RA) of the *Variovorax* genus within the full SynCom across the agar, root and shoot fractions.

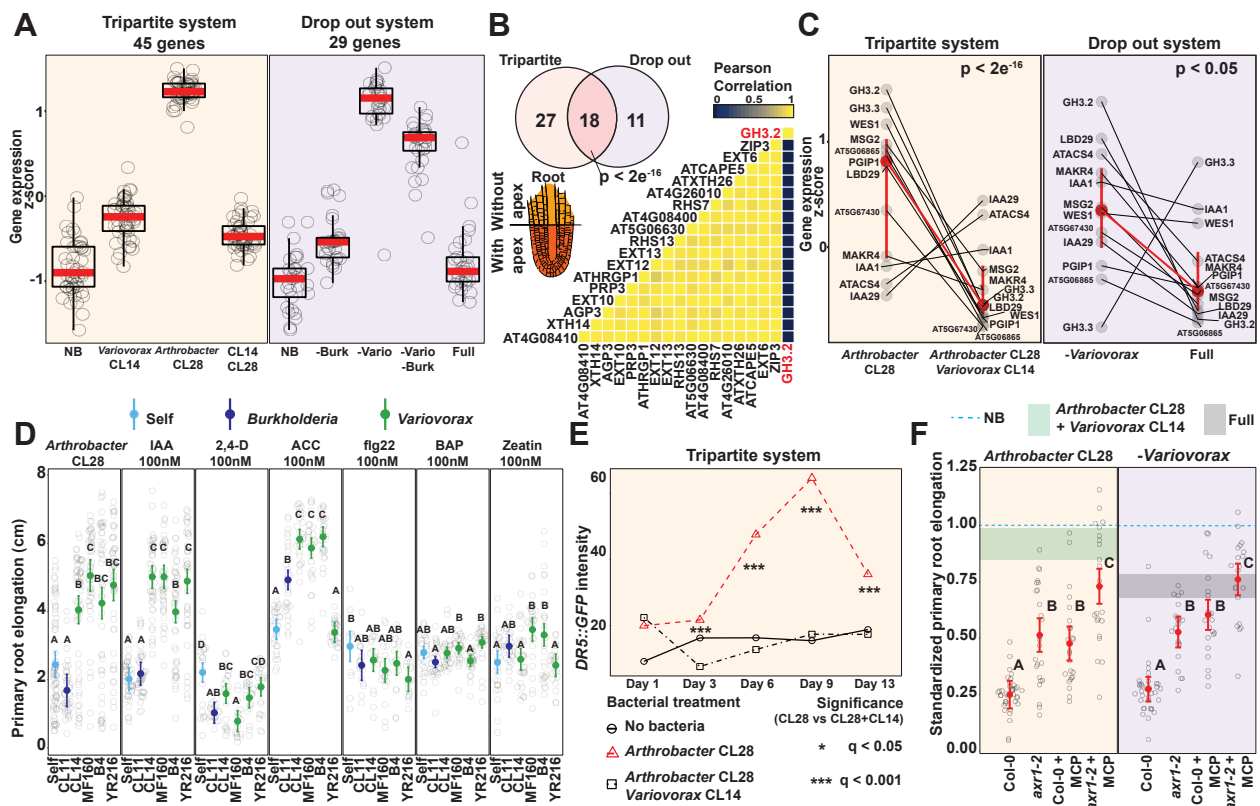


**Fig. 4. *Variovorax* attenuation of root growth inhibition is related to auxin and ethylene signaling.**

**(A)** Boxplots showing the average standardized expression of genes induced in seedlings in response to: Left (Tripartite system) *Arthrobacter* CL28 compared with uninoculated seedlings (NB) or seedlings inoculated with both *Arthrobacter* CL28 and *Variovorax* CL14 (CL14 CL28). Right (Drop-out System) *Variovorax* drop-out SynCom (-Vario) compared to uninoculated seedlings (NB) and to the full SynCom (Full). **(B)** Venn diagram showing the overlap in enriched genes between the tripartite and drop-out systems. The heatmap shows the pairwise correlation in expression of these 18 genes across tissues (14). **(C)** Standardized expression of 12 late-responsive auxin genes across the tripartite and drop-out systems. Each dot represents a gene. Identical genes are connected between bacterial treatments with a black line. Mean expression (95% CI intervals) of the aggregated 12 genes in each treatment is highlighted in red and connected between bacterial treatments with a red line. **(D)** Primary root elongation of seedlings grown with six hormone or MAMP RGI treatments (panels) individually (Self) or with either *Burkholderia* CL11 or four *Variovorax* isolates. Significance between the bacterial treatments is shown using the confidence letter display. **(E)** GFP intensity of *DR5::GFP* *Arabidopsis* seedlings grown with no bacteria, *Arthrobacter* CL28 and *Arthrobacter* CL28+*Variovorax* CL14. Significance within time points is denoted with asterisks. **(F)** Primary root elongation, standardized to sterile conditions, of wild type (Col-0) auxin unresponsive (*axr1-2*), ethylene unresponsive (Col-0 + MCP), or auxin/ethylene unresponsive (*axr1-2* + MCP) seedlings inoculated with RGI-inducing *Arthrobacter* CL28 or the *Variovorax* dropout SynCom (-*Variovorax*). The blue dotted line marks the relative mean length of uninoculated seedlings. The horizontal shade in each panel corresponds to the interquartile range of seedlings (all genotypes) grown with: *Arthrobacter* CL28+*Variovorax* CL14, or the full 185-member SynCom including 10 *Variovorax* isolates (Full SynCom). Differences between treatments are denoted using the compact letter display.

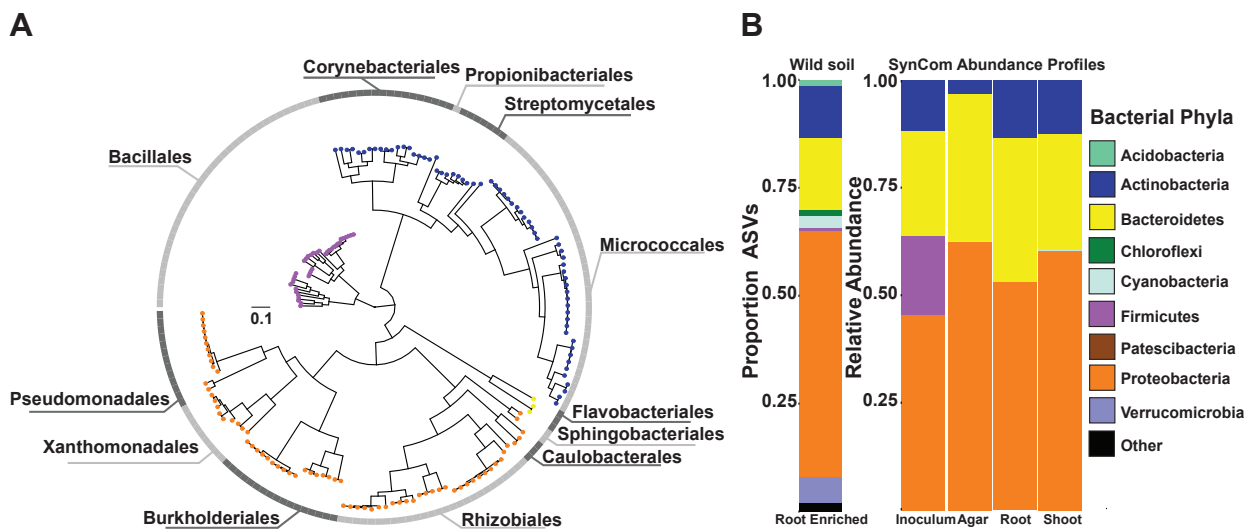


**Fig. S1.**

**Synthetic community resembles the taxonomic makeup of natural communities.**

(A) Phylogenetic tree of 185 bacterial genomes included in the synthetic community (SynCom). The tree tips are colored according to phylum. The outer ring shows the distribution of the 12 distinct bacterial orders present in the SynCom. (B) The panel on the left (wild soil) shows the proportion of amplicon sequence variants (ASVs) enriched ( $q\text{-value} < 0.1$ ) in the plant root in comparison to soil in a microbiota profiling study from the same soil that SynCom strains were isolated from (2). In the panel, ASVs are colored according to phylum. The panel on the right (SynCom panel) represents the relative abundance profiles of bacterial isolates across the initial inoculum, planted agar, root and shoot in plant exposed to the full SynCom. Bacterial isolates in the SynCom are colored based on their phylum.

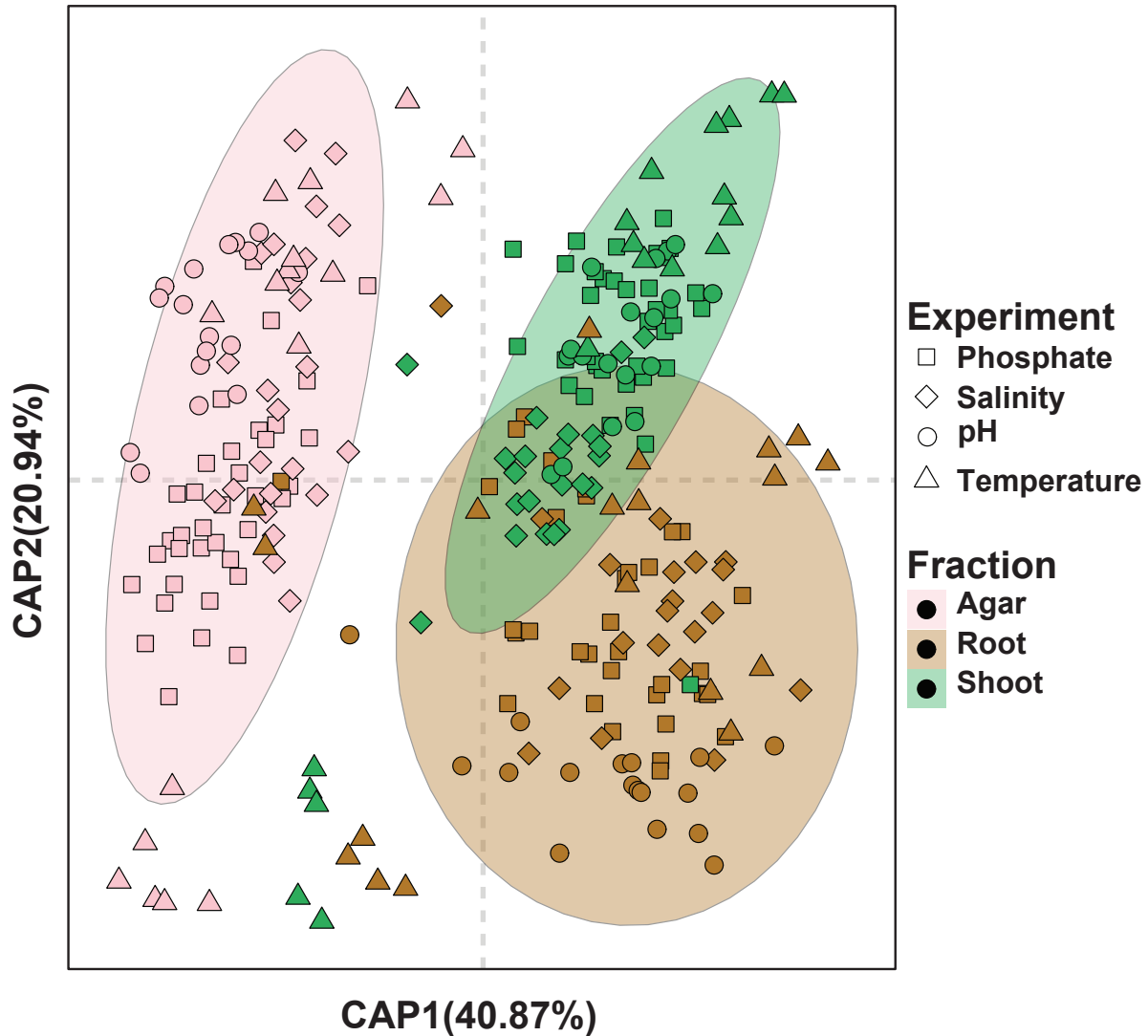


**Fig. S2.**

**Plant microbiota assembly is robust to environmental variations.**

Canonical analysis of principal coordinates showing the influence of the fraction (agar, root, shoot) on the assembly of the bacterial synthetic community across the four gradients used in this work (phosphate, salinity, pH, temperature). Different colors differentiate between the fractions and different shapes differentiate between experiments. Ellipses denote the 95% confidence level of each fraction.

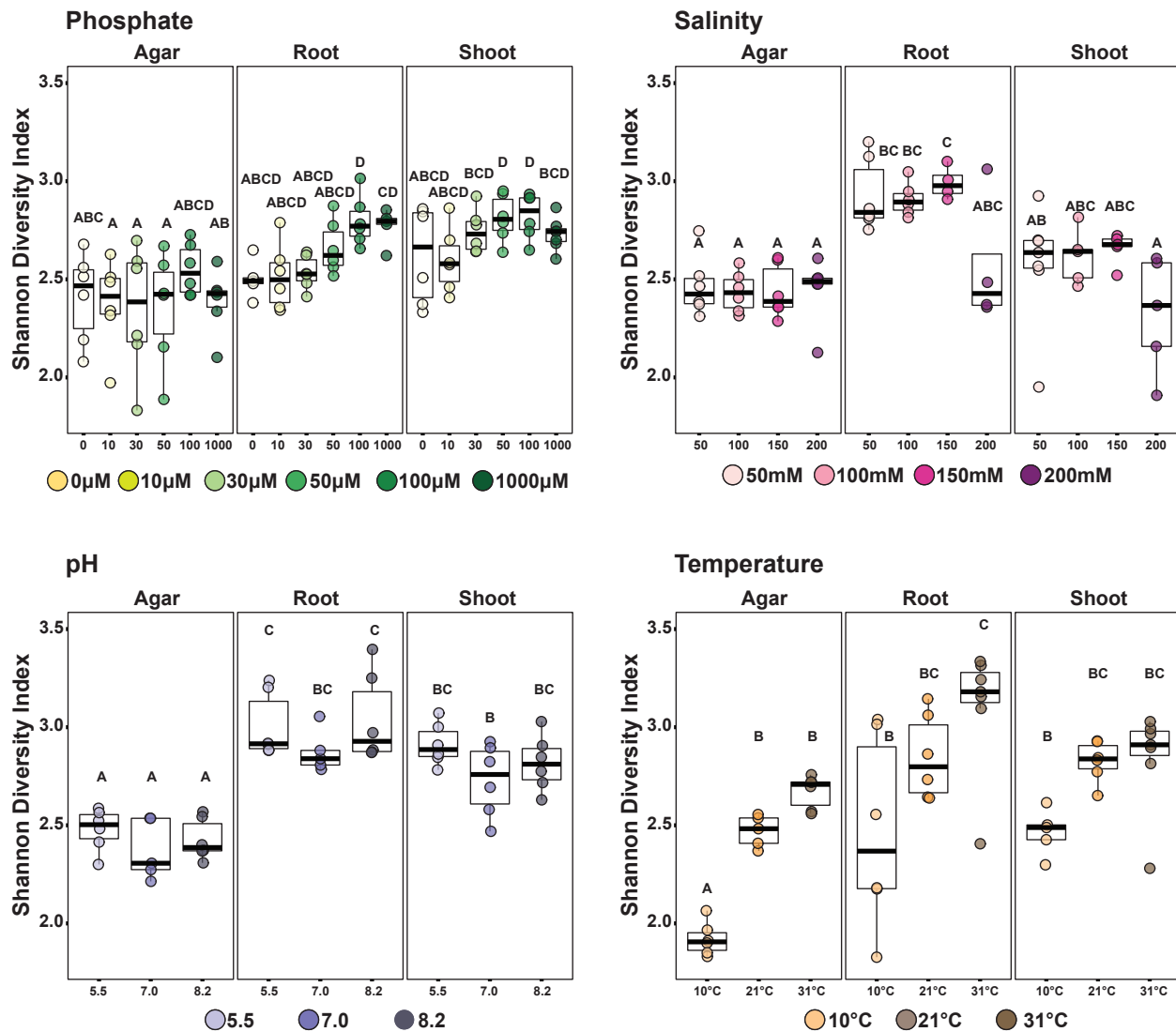


**Fig. S3.**

**Abiotic conditions displayed reproducible effects on alpha-diversity.**

Each panel represents the bacterial alpha-diversity across the different gradient conditions (phosphate, salinity, pH, temperature) and the fractions (agar, root, shoot) used in this work. Bacterial alpha-diversity was estimated using Shannon Diversity. Letters represent the results of the post hoc test of an ANOVA model testing the interaction between fraction and abiotic condition.

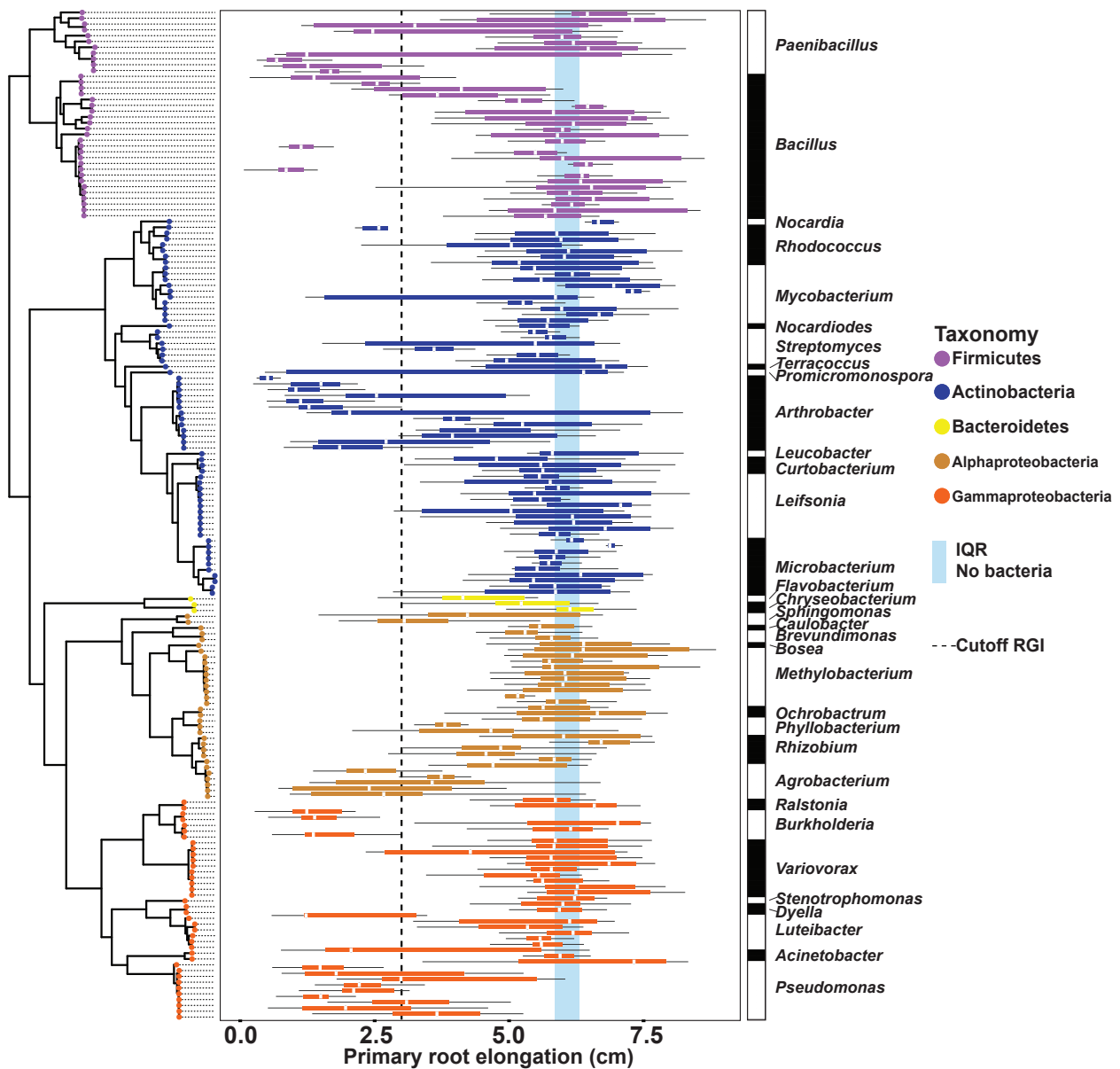


**Fig. S4.**

**Root growth inhibition trait is distributed across bacterial phylogeny.**

Primary root elongation of plants inoculated with single bacterial isolates (one boxplot per isolate). Isolates are ordered according to the phylogenetic tree on the left side of the panel and colored based on their genome-based taxonomy. The vertical blue strips across the panel corresponds to the interquartile range (IQR) of plants grown in sterile conditions. The vertical dotted line represents the 3 cm cutoff used to classify strains as root growth inhibiting strains. The bar on the right side of the panel denotes the genus classification of each isolate.

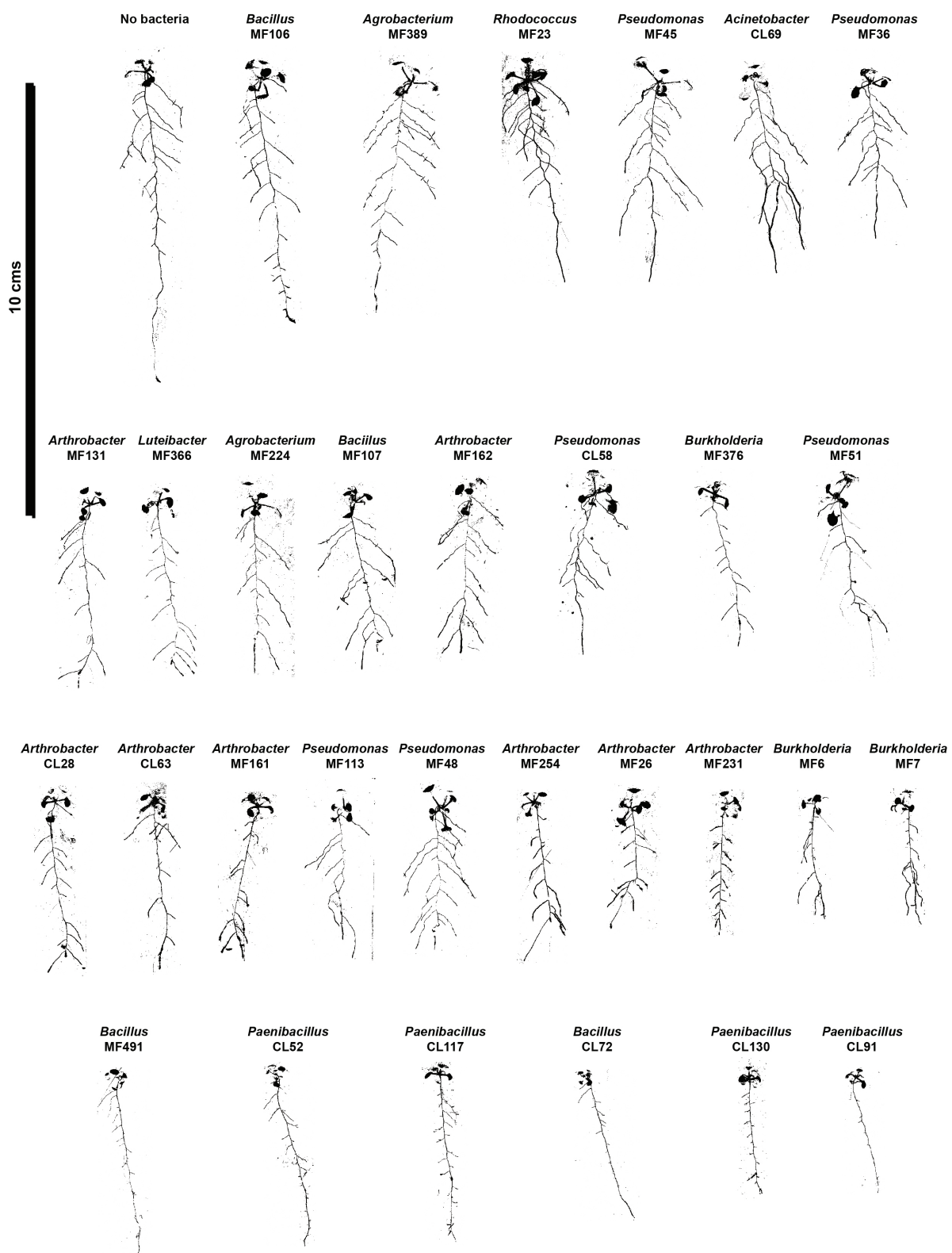


**Fig. S5.**

**Root growth inhibition phenotypes comprise variable root architectures.**

Binarized image of representative seedlings grown axenically (no bacteria) or with thirty-four root growth inhibiting (RGI) strains individually.

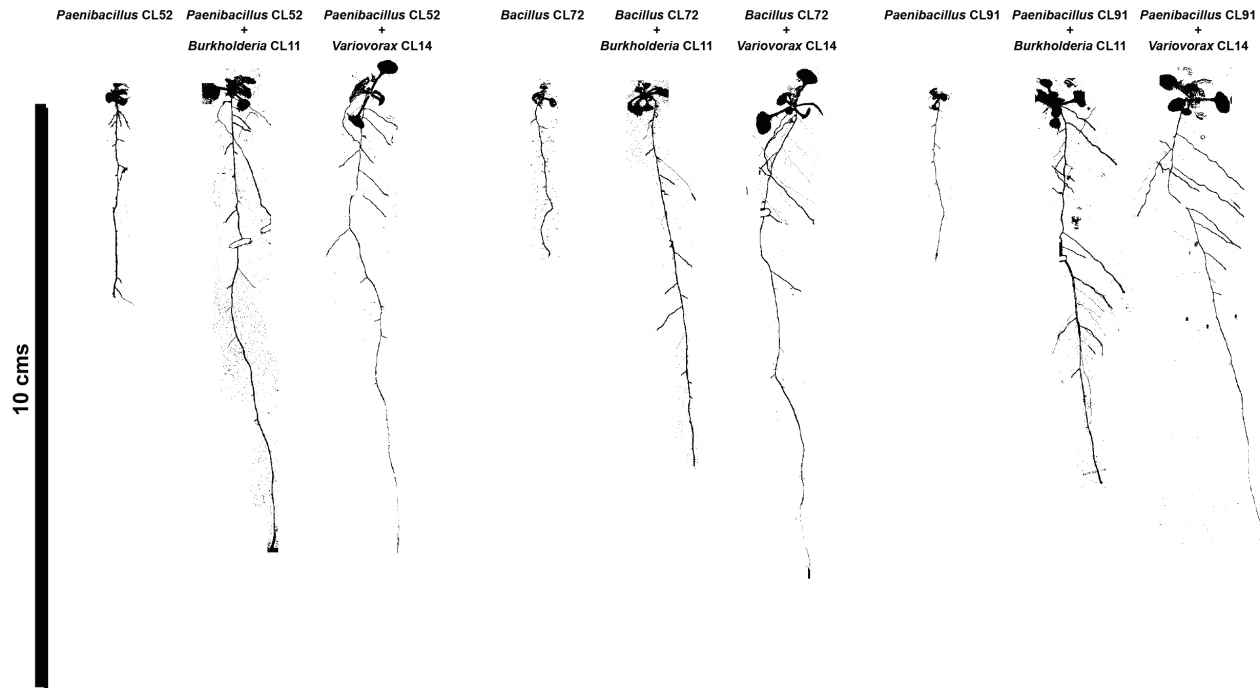


**Fig. S6.**

**Example of strains that attenuate severe root and growth inhibition phenotypes.**

Binarized image of representative seedlings grown with three severely growth inhibiting isolates (*Paenibacillus* CL52, *Bacillus* CL72 and *Paenibacillus* CL91) individually or jointly with *Burkholderia* CL11 or *Variovorax* CL14.

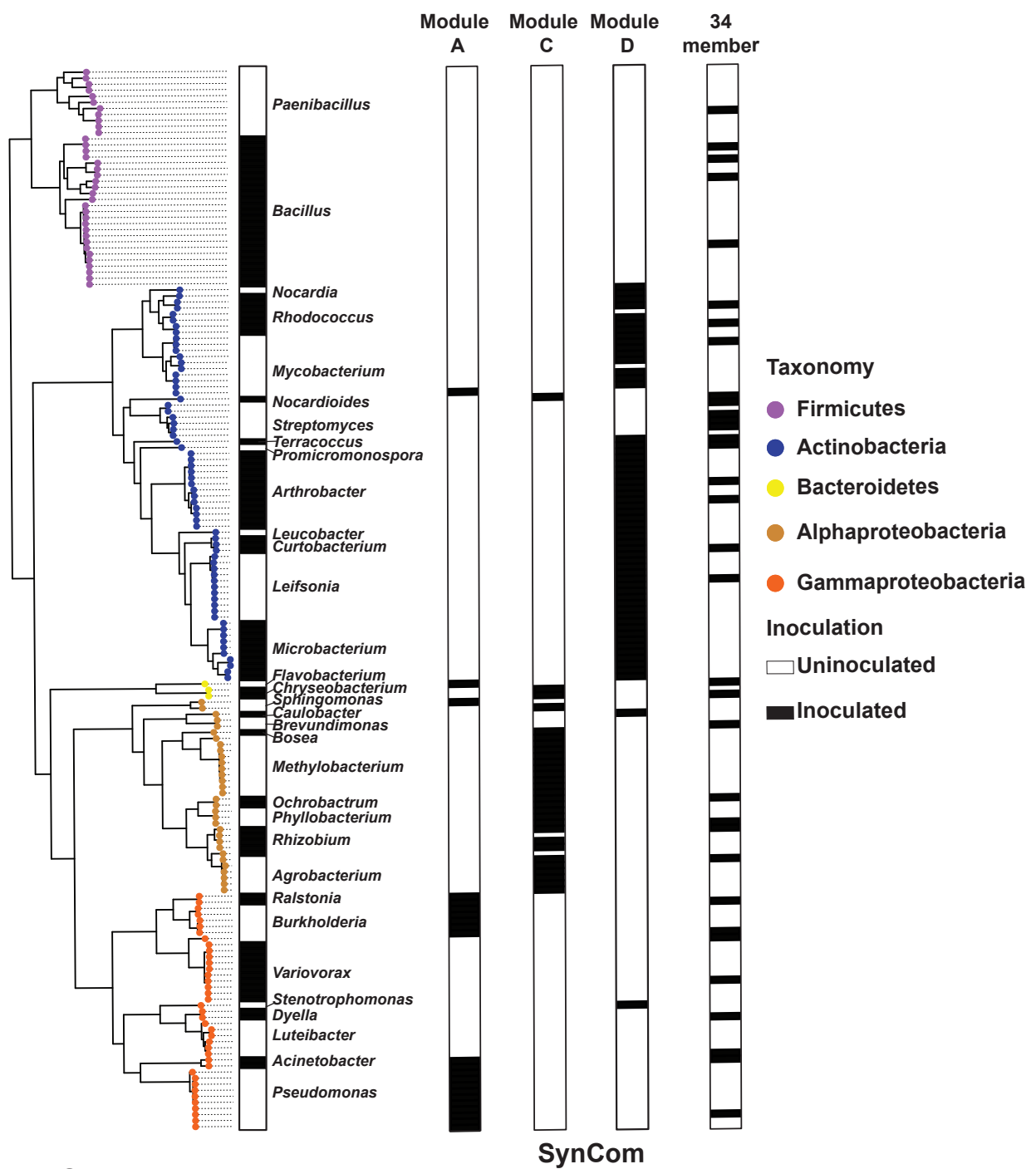


**Fig. S7.**

**Taxonomic composition of the SynCom used in Figure 3D.**

Bar graphs showing the isolate composition of SynComs composed by module A (Module A), module C (Module C), module D (Module D) and a 34-member synthetic community (34 member) (2). Isolates are ordered according to the phylogenetic tree on the left side of the panel. The tips of the phylogenetic tree are colored based on the genome-based taxonomy of each isolate. Presence of an isolate across the different SynComs is denoted by a black filled rectangle.

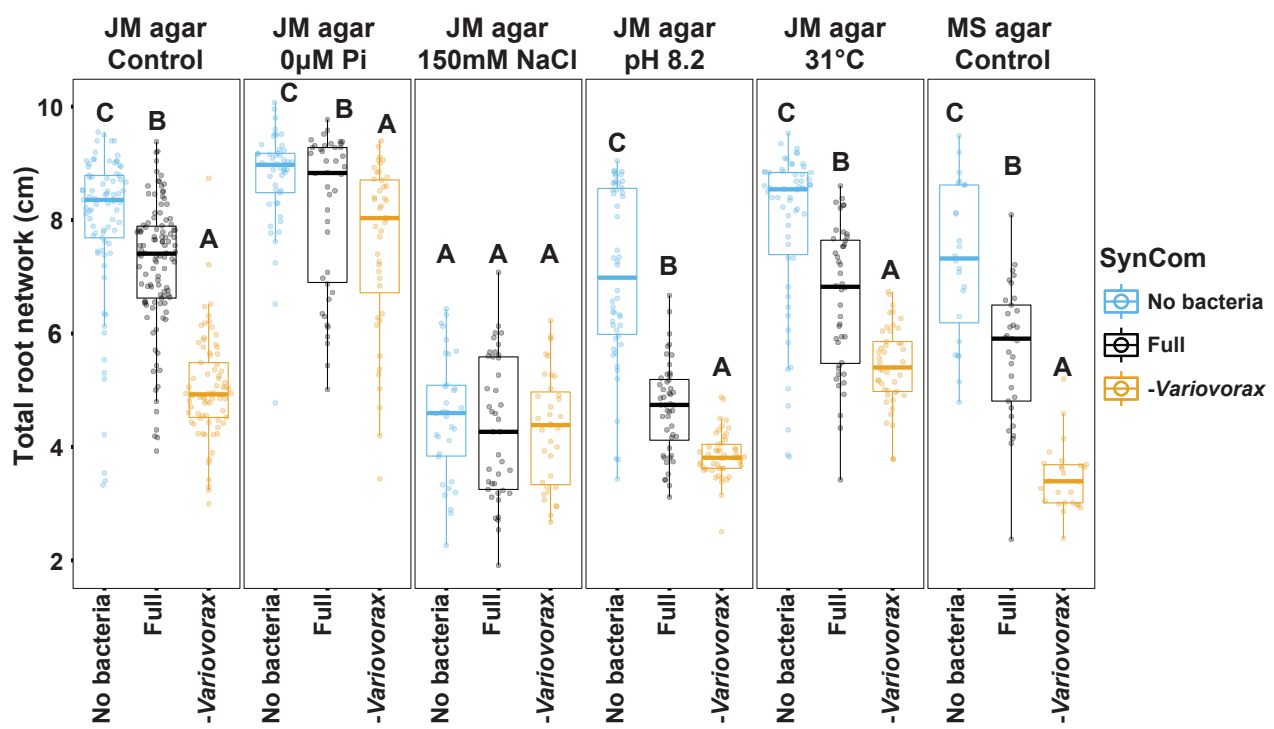


**Fig. S8.**

***Variovorax* increase total root network length.**

Total root network of seedlings grown axenically (No Bacteria), with the full SynCom (Full) or with the full SynCom excluding *Variovorax* (-Variovorax) across different abiotic conditions: full medium (JM agar control), phosphate starvation (JM agar 0 μM Pi), salt stress (JM agar 150 mM NaCl), high pH (JM agar pH 8.2) and high temperature (JM agar 31°C) and media: Johnson medium (JM agar control) and Murashige and Skoog (MS agar control) medium. Letters indicate statistical significance using ANOVA performed within each experimental condition.

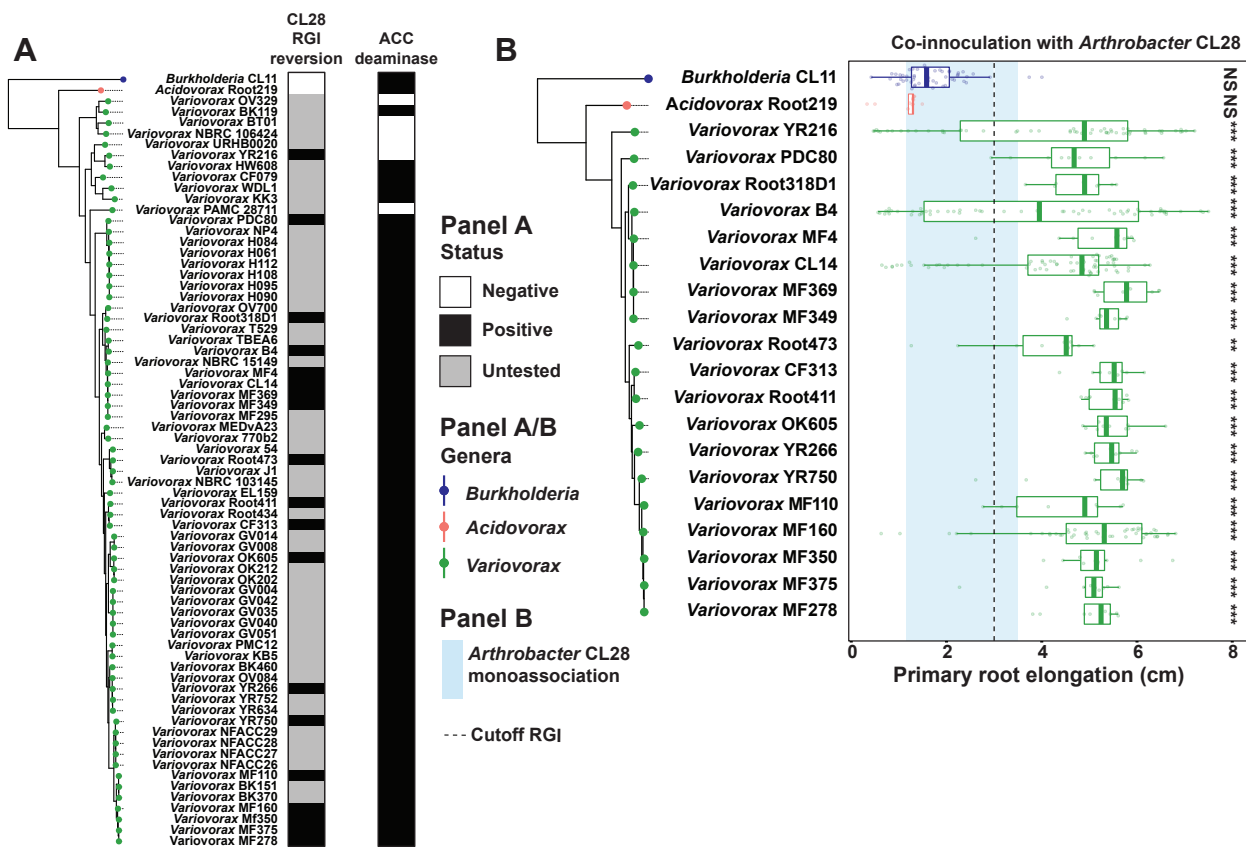


Fig. S9.

**Reversion of root growth inhibition is prevalent across the *Variovorax* phylogeny.**

**(A)** Phylogenetic tree of 54 publicly available *Variovorax* genomes and two outgroup isolates, *Acidovorax* Root219 and *Burkholderia* CL11. The CL28 RGI reversion bar binarizes (positive, negative, untested) the ability of each isolate in the phylogeny to revert the root growth inhibition caused by *Arthrobacter* CL28. The ACC deaminase bar denotes the presence of the KEGG orthology term KO1505 (1-aminocyclopropane-1-carboxylate deaminase) in each of the genomes. **(B)** Phylogenetic tree of 19 *Variovorax* genomes along with two outgroup isolates, *Acidovorax* Root219 and *Burkholderia* CL11 that were tested for their ability to revert the root growth inhibition (RGI) imposed by *Arthrobacter* CL28. The blue vertical strip across the panel denotes the interquartile range of plants treated solely with *Arthrobacter* CL28. The dotted vertical line across the panel denotes the 3 cm cutoff used to classify a treatment as a root growth inhibitor (RGI). Each boxplot is colored according to the genus classification of each isolate. Statistical significance is denoted on the top of each boxplot.

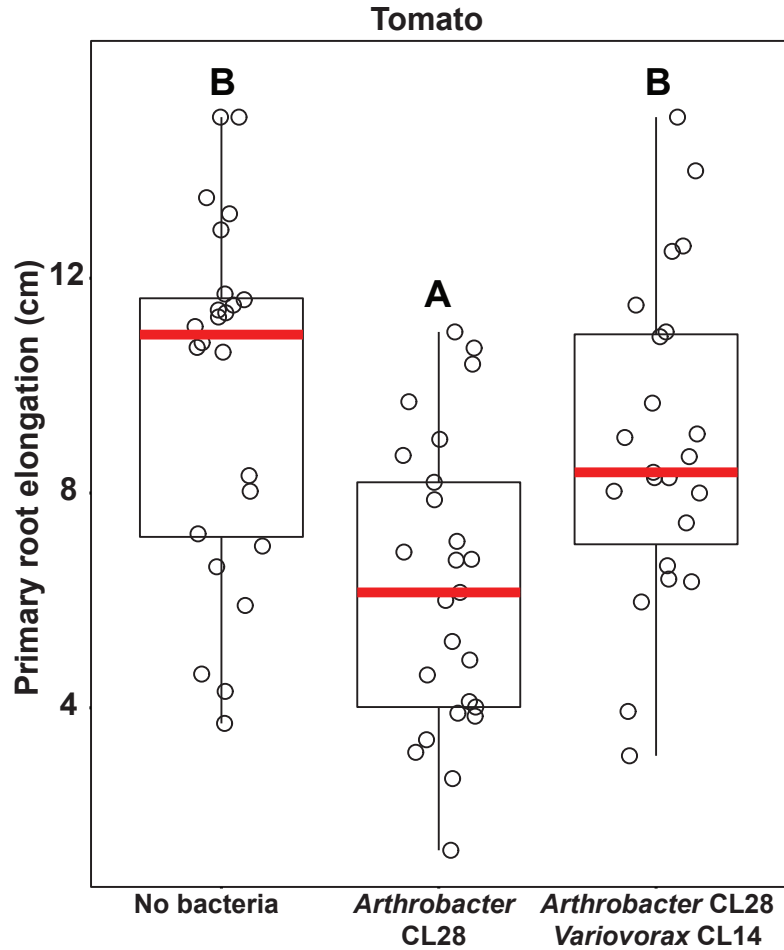
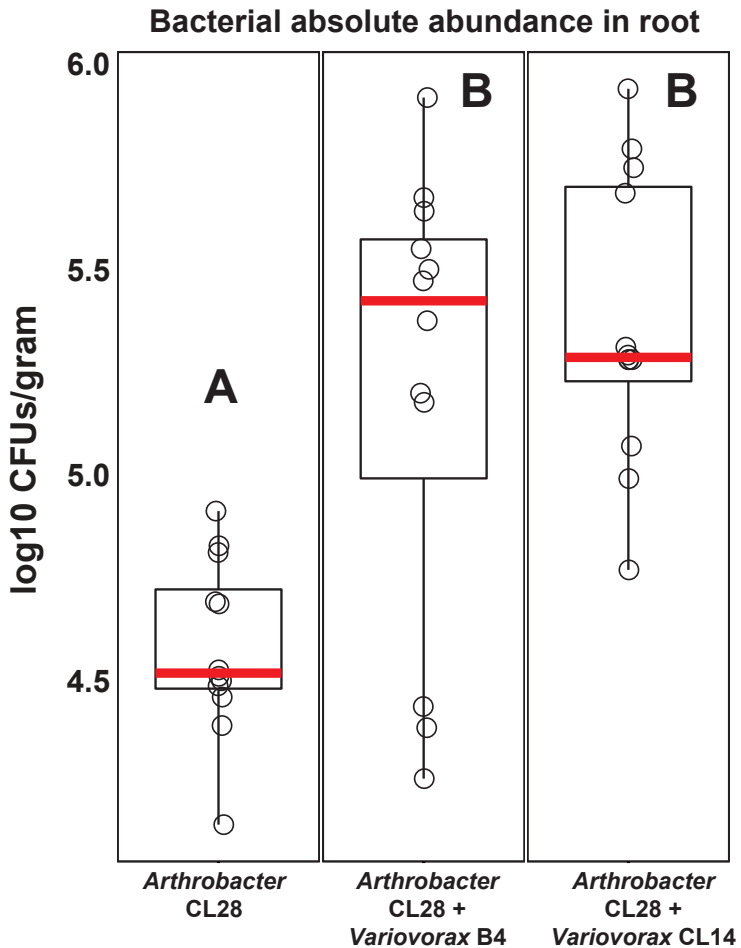


Fig S10.

## Reversion of root growth inhibition in tomato seedlings

Primary root elongation of uninoculated seedlings (No bacteria) or seedlings inoculated with the *Arthrobacter* CL28 individually or along with *Variovorax* CL14. Letters indicate post hoc significance.



**Fig. S11.**

**Variovorax does not inhibit the growth of an RGI strain in *Arabidopsis* roots.**

*In planta* colony forming units of *Arthrobacter* CL28 when inoculated alone or with two *Variovorax* representatives: *Variovorax* B4 and *Variovorax* CL14. Log-transformed-*Colony forming units (CFU)* of *Arthrobacter* CL28 normalized to root weight are shown. To selectively grow *Arthrobacter* CL28, CFUs were counted on Luria Bertani (LB) agar plates containing 50  $\mu$ g/ml of Apramycin, on which neither *Variovorax* B4 and *Variovorax* CL14 grow.

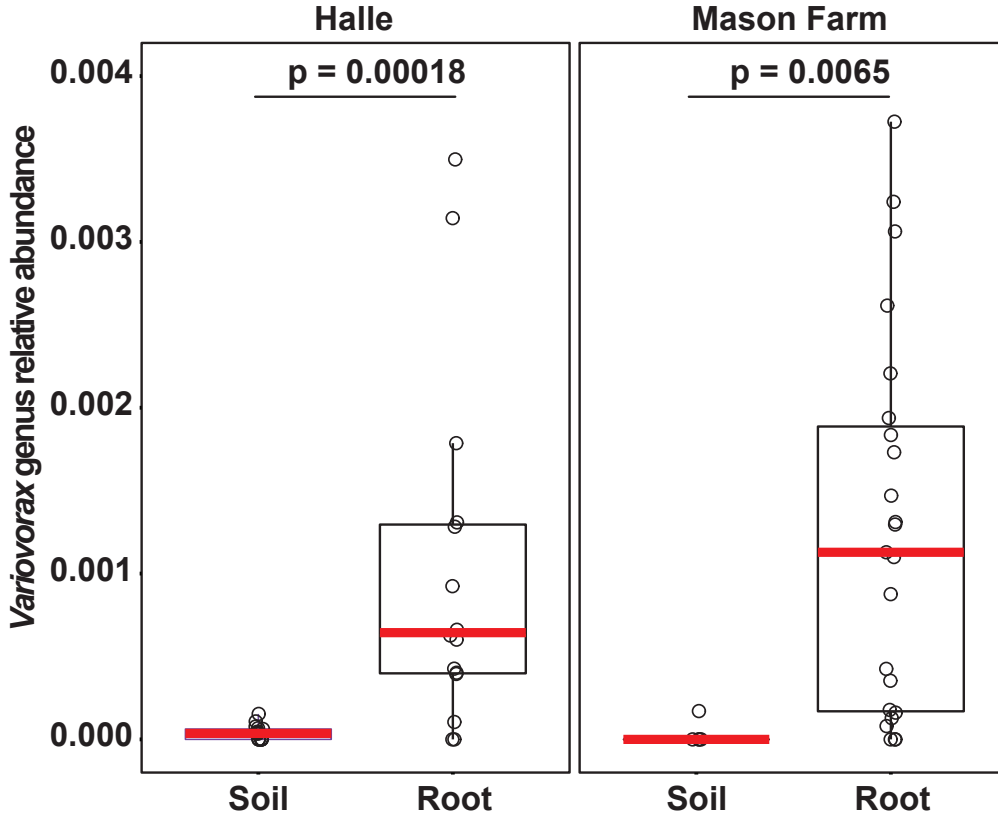


**Fig. S12.**

**Variovorax is a root-enriched taxon.**

Cumulative relative abundance of Amplicon Sequence Variants (ASVs) classified as *Variovorax* across the soil and root fractions of *Arabidopsis thaliana* plants sampled across two independent studies (2,25). The cumulative abundance between fractions was compared using Mann-Whitney U test inside each of the two data sets independently.

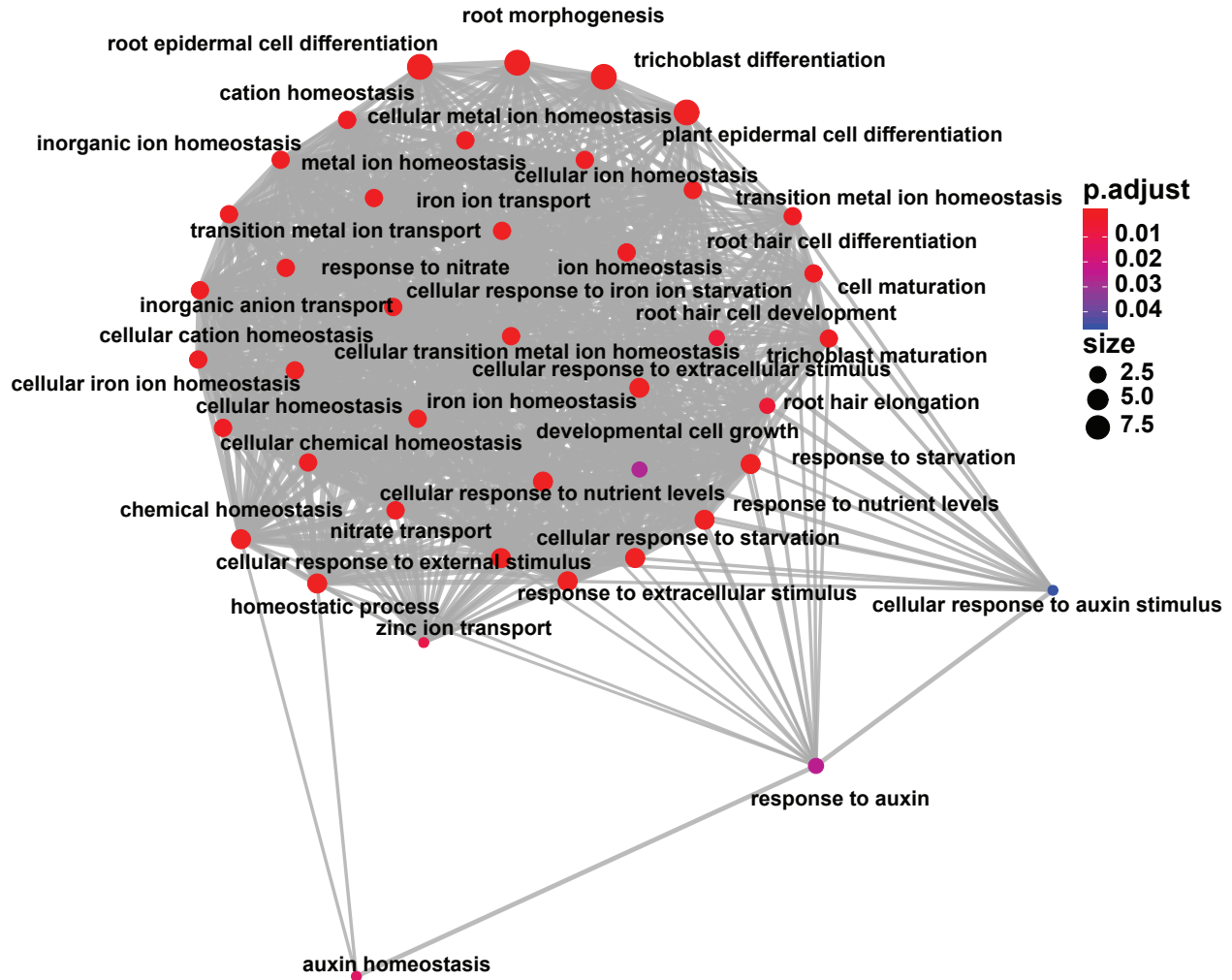


**Fig. S13.**  
**Root growth inhibition-related genes are interconnected.**

Network of statistically significant gene ontology terms contained in the 18 genes cohesively overexpressed in RGI treatments in the tripartite and dropout systems. See Figure 4A and 4B. The network was computed using the emapplot function from the package clusterProfiler in R. A p-value for terms across the gene ontology was computed using a hypergeometric test, additionally the size of each point (Gene ontology term) denotes the number of genes mapped in that particular term.

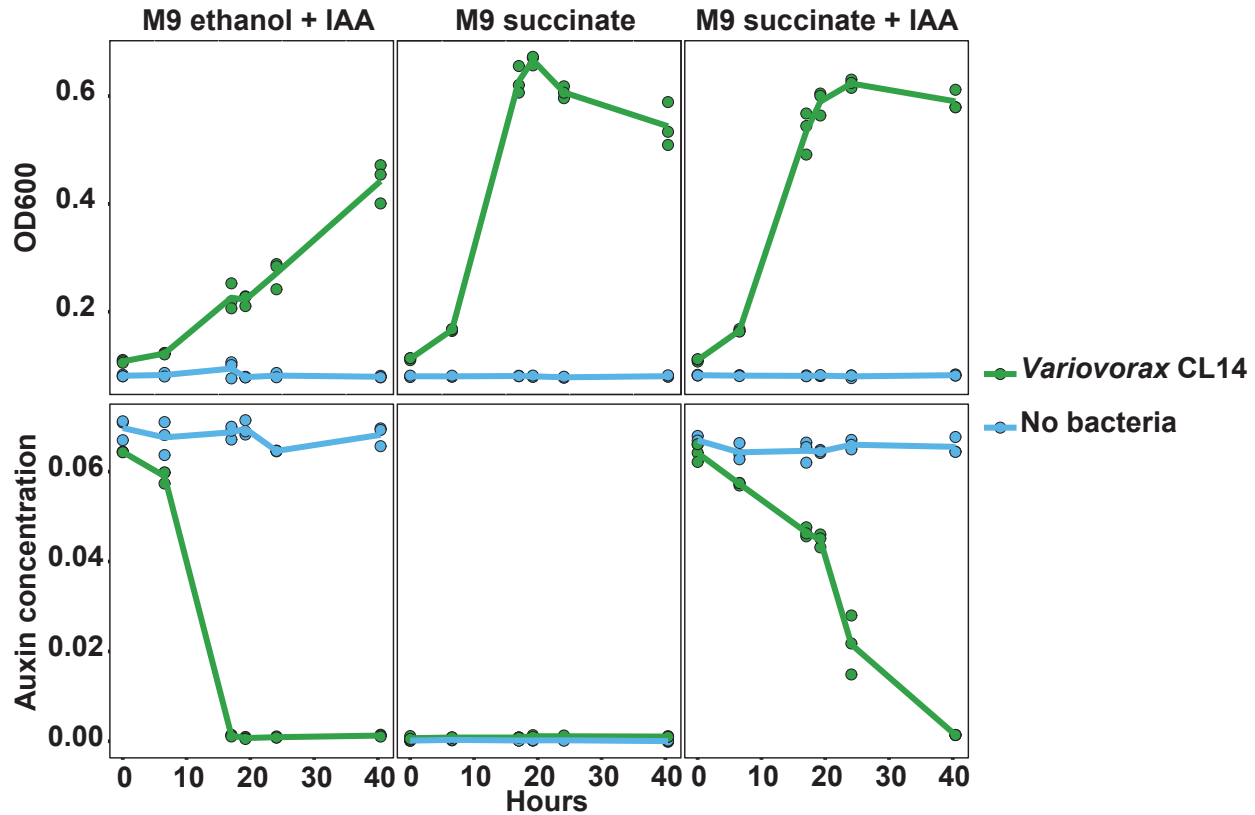


**Fig. S14.**

**Variovorax degrades Indole-3-acetic acid.**

Growth curves showing optical density (OD<sub>600</sub>) (top) and Indole-3-acetic acid (IAA) concentrations (mg/mL) (bottom) in *Variovorax CL14* cultures grown in M9 media with auxin (left), in M9 media with succinate (center) and M9 media with succinate and auxin (right).

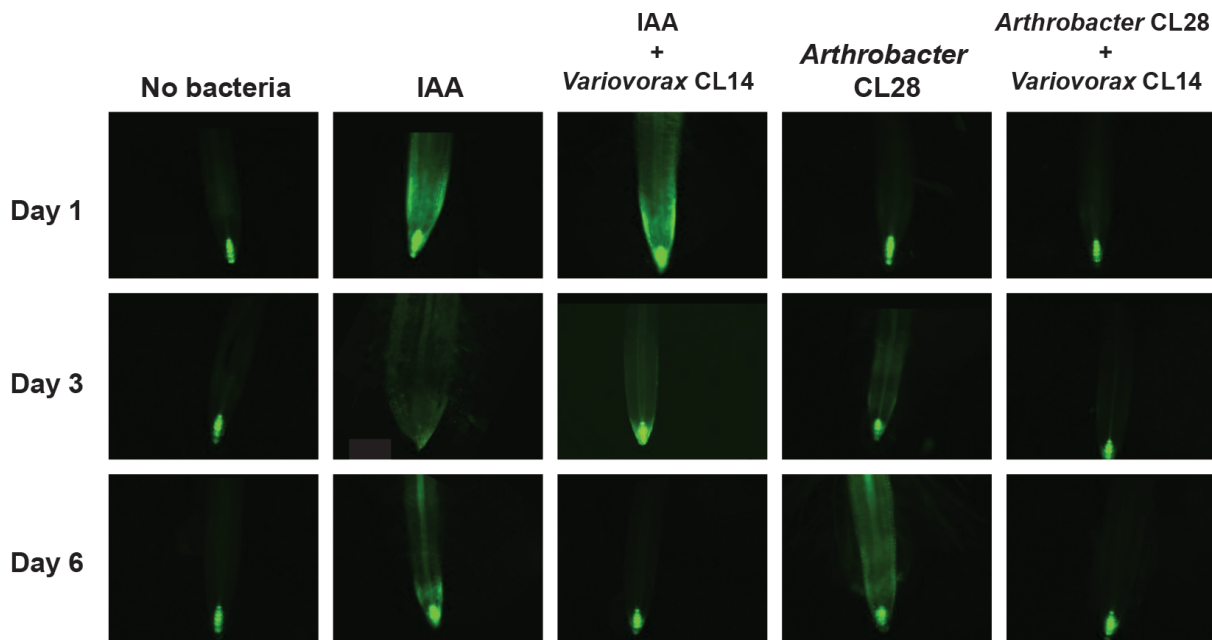


**Fig. S15.**  
***Variovorax* quenches *DR5::GFP* induction.**

Main root tips of plants grown with different Indole-3-acetic acid (IAA) and bacterial treatments. *DR5::GFP* plants were treated with the tripartite system (*Arthrobacter* CL28, *Variovorax* CL14, CL28+CL14), IAA and IAA+*Variovorax* CL14, and GFP fluorescence was imaged 1, 3 and 6 days post inoculation. Fluorescence was quantified in the root elongation zone.

196 **Materials and Methods**

197 **1. *Arabidopsis* with bacterial SynCom microcosm across four stress gradients (Fig. 1, fig. S2-S3, data S2)**

199 **a. Bacterial culture and plant-inoculation**

200 The 185-member bacterial synthetic community (SynCom) used here contains genome-  
201 sequenced isolates obtained from *Brassicaceae* roots, nearly all *Arabidopsis thaliana*, planted in  
202 two North Carolina, US, soils. A detailed description of this collection and isolation procedures  
203 can be found in (25). One week prior to each experiment, bacteria were inoculated from glycerol  
204 stocks into 600  $\mu$ L KB medium in a 96 deep well plate. Bacterial cultures were grown at 28 °C,  
205 shaking at 250 rpm. After five days of growth, cultures were inoculated into fresh media and  
206 returned to the incubator for an additional 48 hours, resulting in two copies of each culture, 7 days  
207 old and 48 hours old. We adopted this procedure to account for variable growth rates of different  
208 SynCom members and to ensure that non-stationary cells from each strain were included in the  
209 inoculum. After growth, 48-hour and 7-day plates were combined and optical density of cultures  
210 was measured at 600 nm (OD<sub>600</sub>) using an Infinite M200 Pro plate reader (TECAN). All cultures  
211 were then pooled while normalizing the volume of each culture to OD<sub>600</sub>=1. The mixed culture  
212 was washed twice with 10 mM MgCl<sub>2</sub> to remove spent media and cell debris and vortexed  
213 vigorously with sterile glass beads to break up aggregates. OD<sub>600</sub> of the mixed, washed culture  
214 was then measured and normalized to OD<sub>600</sub>=0.2. 100  $\mu$ L of this SynCom inoculum was spread  
215 on 10 X 10 cm vertical square agar plates with amended Johnson medium (JM; (2)) without  
216 sucrose prior to transferring seedlings.

217

218 **b. In vitro plant growth conditions**

219 All seeds were surface-sterilized with 70% bleach, 0.2% Tween-20 for 8 min, and rinsed three  
220 times with sterile distilled water to eliminate any seed-borne microbes on the seed surface. Seeds  
221 were stratified at 4 °C in the dark for two days. Plants were germinated on vertical square 10 X  
222 10 cm agar plates with JM containing 0.5% sucrose, for 7 days. Then, 10 plants were transferred  
223 to each of the SynCom-inoculated agar plates. The composition of JM in the agar plates was  
224 amended to produce environmental variation. We added to the previously reported phosphate  
225 concentration gradient (0, 10, 30, 50, 100, 1000  $\mu$ m Pi) (26) three additional environmental  
226 gradients: Salinity (50, 100, 150, 200 mM NaCl), pH (5.5, 7.0, 8.2), Pi concentration and  
227 incubation temperature (10, 21, 31°C). Each gradient was tested separately, in two independent  
228 replicas. Each condition included three SynCom+plant samples, two no plant controls and one no  
229 bacteria control. Plates were placed in randomized order in growth chambers and grown under a

230 16-h dark/8-h light regime at 21 °C day/18 °C night for 12 days. Upon harvest, DNA was extracted  
231 from roots, shoots and agar.

232

233 c. DNA extraction

234 Roots, shoots and agar were harvested separately, pooling 6-8 plants for each sample. Roots  
235 and shoots were placed in 2.0 ml Eppendorf tubes with three sterile glass beads. These samples  
236 were washed three times with sterile distilled water to remove agar particles and weakly  
237 associated microbes. Tubes were stored at -80 °C until processing. Root and shoot samples were  
238 lyophilized for 48 hours using a Labconco freeze dry system and pulverized using a tissue  
239 homogenizer (MPBio). Agar from each plate was stored in 30 ml syringes with a square of  
240 sterilized Miracloth (Millipore) at the bottom and kept at -20 °C for one week. Syringes were then  
241 thawed at room temperature and samples were squeezed gently through the Miracloth into 50 ml  
242 tubes. Samples were centrifuged at max speed for 20 min and most of the supernatant was  
243 discarded. The remaining 1-2 ml of supernatant, containing the pellet, was transferred into clean  
244 microfuge tubes. Samples were centrifuged again, supernatant was removed, and pellets were  
245 stored at -80 °C until DNA extraction. DNA extractions were carried out on ground root and shoot  
246 tissue and agar pellets using 96-well-format MoBio PowerSoil Kit (MOBIO Laboratories; Qiagen)  
247 following the manufacturer's instruction. Sample position in the DNA extraction plates was  
248 randomized, and this randomized distribution was maintained throughout library preparation and  
249 sequencing.

250

251 d. Bacterial 16S sequencing

252 We amplified the V3-V4 regions of the bacterial 16S rRNA gene using the primers 338F (5'-ACT  
253 CCTACGGGAGGCAGCA-3') and 806R (5'-GGACTACHVGGGTWTCTAAT-3'). Two barcodes  
254 and six frameshifts were added to the 5' end of 338F and six frameshifts were added to the 806R  
255 primers, based on the protocol in (27). Each PCR reaction was performed in triplicate, and  
256 included a unique mixture of three frameshifted primer combinations for each plate. PCR  
257 conditions were as follows: 5 µl Kapa Enhancer, 5 µl Kapa Buffer A, 1.25 µl 5 µM 338F, 1.25 µl  
258 5 µM 806R, 0.375 µl mixed chloroplast rRNA gene-blocking peptide nucleic acids (PNAs; 1:1 mix  
259 of 100 µM plastid PNA and 100 µM mitochondrial PNA (27)), 0.5 µl Kapa dNTPs, 0.2 µl Kapa  
260 Robust Taq, 8 µl dH2O, 5 µl DNA; temperature cycling: 95°C for 60 s, 24 cycles of 95°C for 15 s,  
261 78°C (PNA) for 10 s, 50°C for 30 s, 72°C for 30 s, 4°C until use. Following PCR cleanup, the PCR  
262 product was indexed using 96 indexed 806R primers with the same reaction mix as above, and 9  
263 cycles of the cycling conditions described in (2). PCR products were purified using AMPure XP

264 magnetic beads (Beckman Coulter) and quantified with a Qubit 2.0 fluorometer (Invitrogen).  
265 Amplicons were pooled in equal amounts and then diluted to 10 pM for sequencing. Sequencing  
266 was performed on an Illumina MiSeq instrument using a 600-cycle V3 chemistry kit. DNA  
267 sequence data for this experiment is available at the NCBI bioproject repository (accession  
268 PRJNA543313). The abundance matrix, metadata and taxonomy are available at  
269 <https://github.com/isaig/variivoraxRGI>.

270

271 e. 16S amplicon sequence data processing

272 SynCom sequencing data were processed with MT-Toolbox (28). Usable read output from MT-  
273 Toolbox (that is, reads with 100% correct primer and primer sequences that successfully merged  
274 with their pair) were quality filtered using Sickle (29) by not allowing any window with Q-score  
275 under 20. The resulting sequences were globally aligned to a reference set of 16S rDNA  
276 sequences extracted from genome assemblies of SynCom members. For strains that did not have  
277 an intact 16S rDNA sequence in their assembly, we sequenced the 16S rRNA gene using Sanger  
278 sequencing. The reference database also included sequences from known bacterial  
279 contaminants and *Arabidopsis* organellar sequences. Sequence alignment was performed with  
280 USEARCH v7.1090 (30) with the option ‘usearch\_global’ at a 98% identity threshold. On average,  
281 85% of sequences matched an expected isolate. Our 185 isolates could not all be distinguished  
282 from each other based on the V3-V4 sequence and were thus classified into 97 unique sequences  
283 (USeqs). A USeq encompasses a set of identical (clustered at 100%) V3-V4 sequences coming  
284 from a single or multiple isolates.

285

286 Sequence mapping results were used to produce an isolate abundance table. The remaining  
287 unmapped sequences were clustered into Operational Taxonomic Units (OTUs) using UPARSE  
288 (31) implemented with USEARCH v7.1090, at 97% identity. Representative OTU sequences were  
289 taxonomically annotated with the RDP classifier (32) trained on the Greengenes database (33) (4  
290 February 2011; Supplementary Data set 1). Matches to *Arabidopsis* organelles were discarded.  
291 The vast majority of the remaining unassigned OTUs belonged to the same families as isolates  
292 in the SynCom. We combined the assigned USeq and unassigned OTU count tables into a single  
293 count table. In addition to the raw count table, we created rarefied (1000 reads per sample) and  
294 relative abundance versions of the abundance matrix for further analyses.

295

296 The resulting abundance tables were processed and analyzed with functions from the ohchibi  
297 package (<https://github.com/isaig/ohchibi>). An alpha diversity metric (Shannon diversity) was

298 calculated using the diversity function from the vegan package v2.5-3 (34). We used ANOVA to  
299 test for differences in alpha diversity between groups. Beta diversity analyses (Principal  
300 coordinate analysis, and canonical analysis of principal coordinates) were based on Bray-Curtis  
301 dissimilarity calculated from the relative abundance matrices. We used the capscale function from  
302 the vegan R package v.2.5-3 (34) to compute the canonical analysis of principal coordinates  
303 (CAP). To analyze the full dataset (all fraction, all abiotic treatments), we constrained by fraction  
304 and abiotic treatment while conditioning for the replica and experiment effect. We explored the  
305 abiotic conditions effect inside each of the four abiotic gradients tested (phosphate, salinity, pH  
306 and temperature). We performed the Fraction:abiotic interaction analysis within each fraction  
307 independently, constraining for the abiotic conditions while conditioning for the replica effect. In  
308 addition to CAP, we performed Permutational Multivariate Analysis of Variance (PERMANOVA)  
309 using the adonis function from the vegan package v2.5-3 (34). We used the package DESeq2  
310 v1.22.1 (35) to compute the enrichment profiles for USeqs present in the count table.

311  
312 We estimated the fraction effect across all the abiotic conditions tested by creating a group  
313 variable that merged the fraction variable and the abiotic condition variable together (e.g  
314 Root\_0Pi, Agar\_0Pi). We fitted the following model specification using this group variable:  
315 Abundance ~ Rep + Experiment + group

316 From the fitted model, we extracted, for all levels within the group variables, the following  
317 comparisons: Agar vs Root and Agar vs Shoot. A USeq was considered statistically significant if  
318 it had a false discovery rate (FDR) adjusted *p*-value < 0.05.

319  
320 All scripts and dataset objects necessary to reproduce the synthetic community analyses are  
321 deposited in the following github repository: <https://github.com/isaisg/variivoraxRGI>

322  
323 f. Co-occurrence analysis  
324 The relative abundance matrix (USeqs X Samples) was standardized across the USeqs by  
325 dividing the abundance of each USeq in its sample over the mean abundance of that USeq across  
326 all samples. Subsequently, we created a dissimilarity matrix based on the Pearson correlation  
327 coefficient between all the pairs of strains in the transformed abundance matrix, using the cor  
328 function in the stats base package in R. Finally, hierarchical clustering (method ward.D2, function  
329 hclust) was applied over the dissimilarity matrix constructed above.

330  
331 g. Heatmap and family enrichment analysis

332 We visualized the results of the GLM model testing the fraction effects across each specific abiotic  
333 condition tested using a heatmap. The rows in the heatmap were ordered according to the  
334 dendrogram order obtained from the USEqs co-occurrence analysis. The heatmap was colored  
335 based on the log2FoldChange output by the GLM model. We highlighted in a black shade the  
336 comparisons that were significant ( $q\text{-value} < 0.05$ ). Finally, for each of the four modules we  
337 computed for each family present in that module a hypergeometric test testing if that family was  
338 overrepresented (enriched) in that particular module. Families whose FDR p-value  $< 0.1$  were  
339 visualized in the figure.

340

341 **2. Deconstructing the SynCom to four modules of co-occurring strains (Fig. 2A, 2C and**  
342 **data S3).**

343 a. Bacterial culture and plant-inoculation

344 Strains belonging to each module (A, B, C and D, Materials and Methods 1f) were grown in  
345 separate deep 96-well plates and mixed as described above (Materials and Methods 1a). The  
346 concentration of each module was adjusted to OD=0.05 (1/4 of the concentration of the full  
347 SynCom). Each module was spread on the plates either separately, or in combination with  
348 another module. In addition, we included a full SynCom control and an uninoculated control,  
349 bringing the number of SynCom combinations to 12. We performed the experiment in two  
350 independent replicates and each replicate included five plates per SynCom combination.

351

352 b. In vitro plant growth conditions

353 Seed sterilization and germination conditions were the same as Materials and Methods 1b. Plants  
354 were transferred to each of the SynCom-inoculated agar plates containing JM without sucrose.  
355 Plates were placed in randomized order in growth chambers and grown under a 16-h dark/8-h  
356 light regime at 21 °C day/18 °C night for 12 days. Upon harvest, root morphology was measured.

357

358 c. Root and shoot image analysis

359 Plates were imaged twelve days post-transferring, using a document scanner. Primary root length  
360 elongation was measured using ImageJ (36) and shoot area and total root network were  
361 measured with WinRhizo software (Regens Instruments Inc.).

362

363 d. Primary root elongation analyses

364 Primary root elongation was compared across the No Bacteria, full SynCom, single modules and  
365 pairs of modules treatments jointly using an ANOVA model controlling for the replicate effect.

366 Differences between treatments were indicated using the confidence letter display (CLD) derived  
367 from the Tukey's *post hoc* test implemented in the package *emmeans* (37).

368

369

370 **3. Inoculating plants with all SynCom isolates separately (Fig. 2B, fig. S4 and data S4)**

371 a. Bacterial culture and plant-inoculation.

372 Cultures from each strain in the SynCom were grown in KB medium and washed separately, and  
373 OD<sub>600</sub> was adjusted to 0.01 before spreading. We performed the experiment in two independent  
374 replicates and each replicate included one plate per each of the 185 strains. In vitro growth  
375 conditions were the same as in Materials and Methods 2b. Upon harvest, root morphology was  
376 measured (Materials and Methods 2c). Isolates generating an average main root elongation of <3  
377 cm were classified as RGI-inducing strains.

378

379 **4. Tripartite plant-microbe-microbe experiments (Fig. 2D-F and data S5-S6)**

380 a. Experimental design

381 To identify strains that revert RGI (Fig. 2D and data S5), we selected all 18 non-RGI inducing  
382 strains in module A and co-inoculated them with each of four RGI inducing strains, one from each  
383 module. The experiment also included uninoculated controls and controls consisting of each of  
384 the 22 strains inoculated alone, amounting to 95 separate bacterial combinations.

385

386 To confirm the ability of *Variovorax* and *Burkholderia* to attenuate RGI induced by diverse bacteria  
387 (Fig. 2E and data S6), three RGI attenuating strains were co-inoculated with a selection of 18 RGI  
388 inducing strains. The experiment also included uninoculated controls and controls consisting of  
389 each of the 21 strains inoculated alone. Thus, the experiment consisted of 76 separate bacterial  
390 combinations. We performed each of these two experiments in two independent replicates and  
391 each replicate included one plate per each of the strain combinations.

392

393 b. Bacterial culture and plant-inoculation

394 All strains were grown in separate tubes, then washed, and OD<sub>600</sub> was adjusted to 0.02 before  
395 mixing and spreading. In vitro growth conditions were the same as in Materials and Methods 2b.  
396 Upon harvest, root morphology was measured (Materials and Methods 2c) and plant RNA was  
397 harvested and processed from uninoculated samples, and from samples with *Variovorax* CL14,  
398 *Arthrobacter* CL28 and the combination of both (Materials and Methods 4d).

399

400 c. Primary root elongation analysis.  
401 We fitted ANOVA models for each RGI-inducing strain tested. Each model compared the primary  
402 root elongation with the RGI inducing strains alone against root elongation when the RGI inducing  
403 strain was co-inoculated with other isolates. The *p*-values for all the comparisons were corrected  
404 for multiple testing using false discovery rate.

405

406 d. RNA extraction

407 RNA was extracted from *A. thaliana* seedlings following (38). Four seedlings were harvested from  
408 each sample and samples were flash frozen and stored at -80 °C until processing. Frozen  
409 seedlings were ground in liquid nitrogen, then homogenized in a buffer containing 400 µl of Z6-  
410 buffer; 8 M guanidine HCl, 20 mM MES, 20 mM EDTA at pH 7.0. 400 µL  
411 phenol:chloroform:isoamylalcohol, 25:24:1 was added, and samples were vortexed and  
412 centrifuged (20,000 g, 10 minutes) for phase separation. The aqueous phase was transferred to  
413 a new 1.5 ml tube and 0.05 volumes of 1 N acetic acid and 0.7 volumes 96% ethanol were added.  
414 The RNA was precipitated at -20 °C overnight. Following centrifugation (20,000 g, 10 minutes,  
415 4°C), the pellet was washed with 200 µl sodium acetate (pH 5.2) and 70% ethanol. The RNA was  
416 dried and dissolved in 30 µL of ultrapure water and stored at -80 °C until use.

417

418 e. Plant RNA sequencing

419 Illumina-based mRNA-Seq libraries were prepared from 1 µg RNA following (4). mRNA was  
420 purified from total RNA using Sera-mag oligo(dT) magnetic beads (GE Healthcare Life Sciences)  
421 and then fragmented in the presence of divalent cations (Mg<sup>2+</sup>) at 94°C for 6 minutes. The  
422 resulting fragmented mRNA was used for first-strand cDNA synthesis using random hexamers  
423 and reverse transcriptase, followed by second-strand cDNA synthesis using DNA Polymerase I  
424 and RNaseH. Double-stranded cDNA was end-repaired using T4 DNA polymerase, T4  
425 polynucleotide kinase, and Klenow polymerase. The DNA fragments were then adenylated using  
426 Klenow exo-polymerase to allow the ligation of Illumina Truseq HT adapters (D501–D508 and  
427 D701–D712). All enzymes were purchased from Enzymatics. Following library preparation,  
428 quality control and quantification were performed using a 2100 Bioanalyzer instrument (Agilent)  
429 and the Quant-iT PicoGreen dsDNA Reagent (Invitrogen), respectively. Libraries were sequenced  
430 using Illumina HiSeq4000 sequencers to generate 50-bp single-end reads.

431

432 f. RNA-Seq read processing

433 Initial quality assessment of the Illumina RNA-Seq reads was performed using FastQC v0.11.7

434 (39). Trimmomatic v0.36 (40) was used to identify and discard reads containing the Illumina  
435 adaptor sequence. The resulting high-quality reads were then mapped against the TAIR10  
436 Arabidopsis reference genome using HISAT2 v2.1.0 (41) with default parameters. The  
437 featureCounts function from the Subread package (42) was then used to count reads that mapped  
438 to each one of the 27,206 nuclear protein-coding genes. Evaluation of the results of each step of  
439 the analysis was performed using MultiQC v1.1 (43). Raw sequencing data and read counts are  
440 available at the NCBI Gene Expression Omnibus accession number GSE131158.

441

442 **5. *Variovorax* drop-out experiment (Fig. 3A-C and data S7)**

443 a. Bacterial culture and plant-inoculation.

444 The entire SynCom, excluding all 10 *Variovorax* isolates and all five *Burkholderia* isolates was  
445 grown and prepared as described above (Materials and Methods 1a). The *Variovorax* and  
446 *Burkholderia* isolates were grown in separate tubes, washed and added to the rest of the SynCom  
447 to a final OD<sub>600</sub> of 0.001 (the calculated OD<sub>600</sub> of each individual strain in a 185-Member SynCom  
448 at a total of OD<sub>600</sub> of 0.2), to form the following five mixtures: (i) Full community – all *Variovorax*  
449 and *Burkholderia* isolates added to the SynCom; (ii) *Burkholderia* drop-out – only *Variovorax*  
450 isolates added to the SynCom; (iii) *Variovorax* drop-out – only *Burkholderia* isolates added to the  
451 SynCom; (iv) *Variovorax* and *Burkholderia* drop-out – no isolates added to the SynCom; (v)  
452 Uninoculated plants – no SynCom. The experiment consisted of six plates per SynCom mixture,  
453 amounting to 30 plates. Upon harvest, root morphology was measured and analyzed (Materials  
454 and Methods 1c,4c); and Bacterial DNA (Materials and Methods 1d) and plant RNA (Materials  
455 and Methods 4d-e) were harvested and processed.

456

457 **6. *Variovorax* drop-out under varying abiotic contexts (Fig. 3E and data S7)**

458 a. Bacterial culture and plant-inoculation.

459 The composition of JM in the agar plates was amended to produce abiotic environmental  
460 variation. These amendments included salt stress (150 mM NaCl), low Phosphate (10 µm  
461 Phosphate), high pH (pH 8.2) and high temperature (plates incubated at 31 °C), as well as an un-  
462 amended JM control. Additionally, we tested a different media (1/2-strength Murashige and Skoog  
463 [MS]) and a soil-like substrate. As a soil-like substrate, we used calcined clay (Diamond Pro),  
464 prepared as follows: 100 ml of clay was placed in Magenta GA7 vessels. The vessels were then  
465 autoclaved twice. 40 ml of liquid JM was added to the vessels, with the corresponding bacterial  
466 mixture spiked into the media at a final OD<sub>600</sub> of 5E-4. Four 1-week old seedlings were transferred

467 to each vessel, and vessels were covered with Breath-Easy gas permeable sealing membrane  
468 (Research Products International) to maintain sterility and gas exchange.

469  
470 The entire SynCom, excluding all 10 *Variovorax* isolates was grown and prepared as described  
471 above (Materials and Methods 1a). The *Variovorax* isolates were grown in separate tubes,  
472 washed and added to the rest of the SynCom to a final OD<sub>600</sub> of 0.001 (the calculated OD<sub>600</sub> of  
473 each individual strain in a 185-Member SynCom at an OD<sub>600</sub> of 0.2), to form the following five  
474 mixtures: (i) Full community – all *Variovorax* isolates added to the SynCom; (ii) *Variovorax* drop-  
475 out – no isolates added to the SynCom; (iii) Uninoculated plants – no SynCom.

476  
477 We inoculated all three SynCom combinations in all seven abiotic treatments, amounting to 21  
478 experimental conditions. We performed the experiment in two independent replicates and each  
479 replicate included three plates per experimental conditions, amounting to 63 plates per replicate.  
480 Upon harvest, root morphology was measured (Materials and Methods 2c); and Bacterial DNA  
481 (Materials and Methods 1c-e) and plant RNA (Materials and Methods 4d-f) were harvested and  
482 processed, excluding the clay treatment.

483  
484 b. Root image analysis  
485 For agar plates, roots were imaged as described above (Materials and Methods 2c). For calcined  
486 clay pots, four weeks post-transferring, pots were inverted, and whole root systems were gently  
487 separated from the clay by washing with water. Root systems were spread over an empty petri  
488 dish and scanned using a document scanner.

489  
490 c. Primary root elongation and total root network analysis.  
491 Primary root elongation was compared between SynCom treatments within each of the different  
492 abiotic contexts tested independently. Differences between treatments were indicated using the  
493 confidence letter display (CLD) derived from the Tukey's *post hoc* test implemented in the  
494 package emmeans.

495  
496 d. Bacterial 16S data analysis  
497 To be able to compare shifts in the community composition of samples treated with and without  
498 the *Variovorax* genus, we *in silico* removed the 10 *Variovorax* isolates from the count table of  
499 samples inoculated with the Full community treatment. We then merged this count table with the  
500 count table constructed from samples inoculated without the *Variovorax* genus (*Variovorax* drop-

501 out treatment). Then, we calculated a relative abundance of each USeq across all the samples  
502 using the merged count matrix. Finally, we applied Canonical Analysis of Principal Coordinates  
503 (CAP) over the merged relative abundance matrix to control for the replica effect. In addition, we  
504 utilized the function adonis from the vegan R package to compute a PERMANOVA test over the  
505 merged relative abundance matrix and we fitted a model evaluating the fraction and SynCom  
506 (presence of *Variovorax*) effects over the assembly of the community.

507

508 **7. *Variovorax* drop-out under varying biotic contexts (Fig. 3D, fig S7 and data S7)**

509 a. Bacterial culture and plant-inoculation.

510 Strains belonging to modules A (excluding *Variovorax*), C and D were grown in separate wells in  
511 deep 96-well plates and mixed as described above (Materials and Methods 1a). The  
512 concentration of each module was adjusted to OD=0.05 (1/4 of the concentration of the full  
513 SynCom). The *Variovorax* isolates were grown in separate tubes, washed and added to the rest  
514 of the SynCom to a final OD<sub>600</sub> of 0.001.

515

516 In a separate experiment, the 35-member SynCom used in (2) was grown, excluding *Variovorax*  
517 CL14, to create a taxonomically diverse, *Variovorax*-free subset of the full 185 community. The  
518 concentration of this SynCom was adjusted to OD<sub>600</sub>=0.05. The *Variovorax* isolates were grown  
519 in separate tubes, washed and added to the rest of the SynCom to a final OD<sub>600</sub> of 0.001.

520

521 These two experiments included the following mixtures (fig S7 and data S7): (i) Module A  
522 excluding *Variovorax*; (ii) Module C; (iii) Module D; (iv) Module A including *Variovorax*; (v) Module  
523 C + all 10 *Variovorax*; (vi) Module D + all 10 *Variovorax*; (vii) 35-member SynCom excluding  
524 *Variovorax*; (viii) 34-member SynCom + all 10 *Variovorax*; (ix) uninoculated control. The  
525 experiment with modules A, C and D was performed in two independent experiments, with two  
526 plates per treatment in each. The experiment with the 34-member SynCom was performed once,  
527 with 5 plates per treatment. Upon harvest, root morphology was measured (Materials and  
528 Methods 2c).

529

530 b. Primary root elongation analysis.

531 We directly compared differences between the full SynCom and *Variovorax* drop-out treatment  
532 using a *t*-test and adjusting the *p*-values for multiple testing using false discovery rate.

533

534 **8. Phylogenetic inference of the SynCom and *Variovorax* Isolates (Fig 2A, fig. S1A, S4, S7)**

535 **and S9A-B)**

536 To build the phylogenetic tree of the SynCom isolates, we used the super matrix approach  
537 previously described in (25). We scanned 120 previously defined marker genes across the 185  
538 isolate genomes from the SynCom utilizing the hmmsearch tool from the hmmer v3.1b2 (44).  
539 Then, we selected 47 markers that were present as single copy genes in 100% of our isolates.  
540 Next, we aligned each individual marker using MAFFT (45) and filtered low quality columns in the  
541 alignment using trimAI (46). Then, we concatenated all filtered alignments into a super alignment.  
542 Finally, FastTree v2.1 (47) was used to infer the phylogeny utilizing the WAG model of evolution.  
543 For the *Variovorax* relative's tree, we chose 56 markers present as single copy across 124  
544 Burkholderiales isolates and implemented the same methodology described above.

545

546 **9. Measuring how prevalent is the RGI attenuation trait across the *Variovorax* phylogeny**  
547 **(fig. S9A-B, data S1 and data S8)**

548 a. Bacterial culture and plant-inoculation.

549 Fifteen *Variovorax* strains from across the genus' phylogeny were each co-inoculated with the  
550 RGI inducer *Arthrobacter* CL28. All 16 strains were grown in separate tubes, then washed, and  
551 OD<sub>600</sub> was adjusted to 0.01 before mixing. Pairs of strains were mixed in 1:1 ratios and spread  
552 onto agar prior to seedling transfer. The experiment also included uninoculated controls and  
553 controls consisting of each of the 16 strains inoculated alone. Thus, the experiment consisted of  
554 32 separate bacterial combinations. We performed the experiment one time, which included 3  
555 plates per bacterial combination. Upon harvest, root morphology was measured (Materials and  
556 Methods 2c). Primary root elongation was analyzed as described above (Materials and Methods  
557 4c).

558

559 **10. Measuring root growth inhibition in tomato seedlings (fig. S10 and data S9)**

560 a. Experimental design

561 This experiment included the following treatments: (i) No bacteria, (ii) *Arthrobacter* CL28, (iii)  
562 *Variovorax* CL14 and (iv) *Arthrobacter* CL28 + *Variovorax* CL14. Each treatment was repeated in  
563 three separate agar plates with five tomato seedlings per plate. The experiment was repeated in  
564 two independent replicates.

565

566 b. Bacterial culture and plant-inoculation

567 All strains were grown in separate tubes, then washed, and OD<sub>600</sub> was adjusted to 0.01 before  
568 mixing and spreading. 400  $\mu$ L of each bacterial treatment was spread on 20 X 20 agar plates  
569 containing JM agar with no sucrose.

570

571 c. In vitro plant growth conditions

572 We used Heinz 1706 seeds. All seeds were soaked in sterile distilled water for 15 min, then  
573 surface-sterilized with 70% bleach, 0.2% Tween-20 for 15 min, and rinsed five times with sterile  
574 distilled water to eliminate any seed-borne microbes on the seed surface. Seeds were stratified  
575 at 4 °C in the dark for two days. Plants were germinated on vertical square 10 X 10 cm agar plates  
576 with JM containing 0.5% sucrose, for 7 days. Then, 5 plants were transferred to each of the  
577 SynCom-inoculated agar plates. Upon harvest, root morphology was measured. (Materials and  
578 Methods 2c).

579

580 c. Primary root elongation analysis.

581 Differences between treatments were indicated using the confidence letter display (CLD) derived  
582 from the Tukey's *post hoc* test from an ANOVA model.

583

584

## 585 **11. Enumeration of *Arthrobacter* CL28 colony forming units from roots (fig. S11 and data 586 S10)**

587 Arabidopsis seedlings were inoculated with (i) *Arthrobacter* CL28 alone, (ii) *Arthrobacter* CL28 +  
588 *Variovorax* CL14 or (iii) *Arthrobacter* CL28 + *Variovorax* B4, as described above (Material and  
589 Methods 4b). Each bacterial treatment included four separate plates, with nine seedlings in each  
590 plate. Upon harvest, all seedlings were placed in pre-weighed 2.0 ml Eppendorf tubes containing  
591 three glass beads, three seedlings per tube (producing 12 data points per treatment). Roots were  
592 weighed, then crushed using a bead beater. The resulting suspension was plated on Luria Bertani  
593 agar plates containing 50  $\mu$ g/ml of Apramycin, in a dilution series, and colonies were counting  
594 after incubation of 48 hours at 28° C.

595

596

## 597 **12. RNA-Seq analysis (Fig. 4A-C, fig. S13 and data S11-12)**

598 a. Detection of RGI-induced genes (Fig. 4A-B)

599 To measure the transcriptional response of the plant to the different SynCom combinations, we  
600 used the R package DESeq2 v.1.22.1 (35). The raw count genes matrixes for the dropout and

601 tripartite experiments were used independently to define differentially expressed genes (DEGs).  
602 For the analysis of both experiments we fitted the following model specification:  
603 Abundance Gene ~ SynCom  
604 From the fitted models we derived the following contrasts to obtain differentially expressed genes  
605 (DEGs). A gene was considered differentially expressed if it had a  $q$ -value  $< 0.1$ . For the tripartite  
606 system (Materials and Methods 4), we performed the following contrasts: *Arthrobacter* CL28 vs  
607 No Bacteria (NB) and *Arthrobacter* CL28 vs *Arthrobacter* CL28 co-inoculated with *Variovorax*  
608 CL14. The logic behind these two contrasts was to identify genes that were induced in RGI plants  
609 (*Arthrobacter* CL28 vs NB) AND repressed by *Variovorax* CL14. For the dropout system  
610 (Materials and Methods 5), we performed the following contrasts, *Variovorax* drop-out vs NB, and  
611 *Variovorax* drop-out vs full SynCom. The logic behind these two contrasts was identical to the  
612 tripartite system: to identify genes that are associated with the RGI phenotype (*Variovorax* drop-  
613 out vs NB contrast) AND repressed when *Variovorax* are present (*Variovorax* drop-out vs full  
614 SynCom contrast).

615  
616 For visualization purposes, we applied a variance stabilizing transformation to the raw count gene  
617 matrix. We then standardized each gene expression (z-score) along the samples. We subset  
618 DEGs from this standardized matrix and calculated the mean z-score expression value for each  
619 SynCom treatment.

620  
621 To identify the tissue specific expression profile of the 18 intersecting genes between the tripartite  
622 and dropout systems, we downloaded the spatial expression profile of each gene from the  
623 Klepikova atlas (14) using the Bio-analytic resource of plant biology platform. Then, we  
624 constructed a spatial expression matrix of the 18 genes and computed pairwise Pearson  
625 correlation between all pairs of genes. Finally, we applied hierarchical clustering to this correlation  
626 matrix.

627  
628 b. Comparison with acute auxin response dataset (Figure 4C)  
629 We applied a variance stabilizing transformation to the raw count gene matrix. We then  
630 standardized each gene expression (z-score) along the samples. From this matrix, we subset 12  
631 genes that in a previous study (15) exhibited the highest fold change between auxin treated and  
632 untreated samples. Finally, we calculated the mean z-score expression value of each of these 12  
633 genes across the SynCom treatments. We estimated the statistical significance of the trend of  
634 these 12 genes between a pair of SynCom treatments (Full SynCom vs *Variovorax* drop-out,

635 *Arthrobacter* CL28 vs *Arthrobacter* CL28 plus *Variovorax* CL14) using a permutation approach:  
636 we estimated a *p*-value by randomly selecting 12 genes 10000 times from the expression matrix  
637 and comparing the mean expression between the two SynCom treatments (e.g Full SynCom vs  
638 *Variovorax* drop-out) with the actual mean expression value from the 12 genes reported as robust  
639 auxin markers.

640

641 **13. Measuring the ability of *Variovorax* to attenuate RGI induced by small molecules**  
642 **(Figure 4D and data S13)**

643 a. Bacterial culture and plant-inoculation.

644 We embedded each of the following compounds in JM plates: 100 nM IAA, 1 $\mu$ M IAA, 100 nM  
645 ACC, 100 nM 2,4-d, 100 nM flg22, 100 nM BAP and 100 nM Zeatin. Plates with each compound  
646 were inoculate with one of the *Variovorax* strains CL14, MF160, B4 or YR216 or with *Burkholderia*  
647 CL11. These strains were grown in separate tubes, then washed, and OD<sub>600</sub> was adjusted to 0.01  
648 before spreading 100 $\mu$ L on plates. In addition, we included uninoculated controls for each  
649 compound. We also included unamended JM plates inoculated with the RGI inducer *Arthrobacter*  
650 CL28 co-inoculated with each of the *Variovorax/Burkholderia* strains or alone. Thus, the  
651 experiment included 42 individual treatments. The experiment was repeated twice, with three  
652 independent replicates per experiment. Upon harvest, root morphology was measured (Materials  
653 and Methods 2c).

654

655 b. Primary root elongation analysis.

656 Primary root elongation was compared between bacterial treatments within each of root growth  
657 inhibition treatments tested. Differences between treatments were estimated as described above  
658 (Materials and Methods 4c). We plotted the estimated means with 95% CI of each bacterial  
659 treatment across the different RGI treatments.

660

661

662 **14. In vitro growth of *Variovorax* (fig. S14)**

663 *Variovorax* CL14 was grown in 5mL cultures for 40 hours at 28 °C in 1x M9 minimal salts media  
664 (Sigma M6030) supplemented with 2mM MgSO<sub>4</sub>, 0.1mM CaCl<sub>2</sub>, 10 $\mu$ M FeSO<sub>4</sub>, and a carbon  
665 source: either 15mM succinate alone, 0.4mM Indole-3-acetic acid (IAA) with 0.5% Ethanol from  
666 IAA solubilization, or both. Optical density at 600 nm and IAA concentrations were measured at  
667 six time points. IAA concentrations were measured using the Salkowski method modified from  
668 (48). 100 $\mu$ L of Salkowski reagent (10mM FeCl<sub>3</sub> in 35% perchloric acid) was mixed with 50 $\mu$ L

669 culture supernatant or IAA standards and color was allowed to develop for 30 min prior to  
670 measuring the absorbance at 530nm.

671

672 **15. Measuring plant Auxin response *in-vivo* using a bioreporter line (Fig. 4E-F and data  
673 S14)**

674 a. Bacterial culture and plant-inoculation.

675 7-day old transgenic *Arabidopsis* seedlings expressing the *DR5::GFP* reporter construct (49) were  
676 transferred onto plates containing: (i) 100 nM IAA, (ii) *Arthrobacter* CL28, (iii) 100 IAA + *Variovorax*  
677 CL14, (iv) *Arthrobacter* CL28 + *Variovorax* CL14, (v) the *Variovorax* drop-out SynCom, (vi) the  
678 full SynCom, (vii) uninoculated plates. For treatments ii,iii, Bacterial strains were grown in  
679 separate tubes, then washed, and OD<sub>600</sub> was adjusted to 0.01. For treatment iv, OD-adjusted  
680 cultures were mixed in 1:1 ratios and spread onto agar prior to seedling transfer. Cultures for  
681 treatments v and vi were prepared as described above (Materials and Methods 6a).

682 b. Fluorescence microscopy.

683 GFP fluorescence in the root elongation zone of 8-10 plants per treatment were visualized using  
684 a Nikon Eclipse 80i fluorescence microscope at days 1, 3, 6, 9 and 13 post inoculation. The  
685 experiment was performed in two independent replicates.

686 From each root imaged, 10 random 30 X 30 pixel squares were sampled and average GFP  
687 intensity was measured using imageJ (36). Treatments were compared within each time point  
688 using ANOVA tests with Tukey's post hoc in the R base package emmeans. For visualization  
689 purposes we plotted the estimated means of each bacterial across the different timepoints.

690

691 **16. Measuring the dual role of auxin and ethylene perception in SynCom-induced RGI (Fig.  
692 4F and data S15)**

693 a. Bacterial culture and plant-inoculation.

694 We transferred four 7-day old wild type seedling and four *axr1-2* seedlings to each plate in this  
695 experiment. The plates contained one of five bacterial treatments: (i) *Arthrobacter* CL28, (ii)  
696 *Arthrobacter* CL28 + *Variovorax* CL14, (iii) *Variovorax* drop-out SynCom, (iv) Full SynCom, (v)  
697 uninoculated, prepared as described above (Materials and Methods 15a) Plates were placed  
698 vertically inside sealed 86 X 68 cm Ziploc bags. In one of the bags, we placed an open water  
699 container with 80 2.5 gram sachets containing 0.014% 1-MCP (Ethylene Buster, Chrystal  
700 International BV). In the second bag we added, as a control, an open water container. Both bags  
701 were placed in the growth chamber for 12 days. After 6 days of growth, we added 32 additional

702 sachets to the 1-MCP-treated bag to maintain 1-MCP concentrations in the air. Upon harvest, root  
703 morphology was measured (Materials and Methods 2c).

704

705 b. Primary root elongation analysis.

706 Primary root elongation was standardized to the No bacteria control of each genotype, and  
707 compared between genotype/1-MCP treatments within the *Arthrobacter* CL28 treatment and the  
708 *Variovorax* drop-out SynCom treatment, independently. Differences between treatments were  
709 estimated as described above (Materials and Methods 4c). We plotted the estimated means with  
710 95% CI of each bacterial treatment across the four genotypes. We calculated the interquartile  
711 range for the Full and *Arthrobacter* CL28/*Variovorax* CL14 treatments pooling the four  
712 genotypes/treatments.

713

714

## 715 **17. Preparation of binerized plant images (Fig 2C, 3B and fig. S5-S6)**

716 To present representative root images, we increased contrast and subtracted background in  
717 imageJ, then cropped the image to select representative roots. Neighboring roots were manually  
718 erased from the cropped image.

719

## 720 **18. Mining *Variovorax* genomes for auxin degradation operons and ACC-deminase genes 721 (Discussion).**

722 We used local alignment (BLASTp) to search for the presence of the 10 genes (*iacA*, *iacB*, *iacC*,  
723 *iacD*, *iacE*, *iacF*, *iacG*, *iacH*, *iacI*, and *iacY*) of a previously characterized auxin degradation  
724 operon (50) across the 10 *Variovorax* isolates in our bacterial synthetic community and searched  
725 for hotspots of clustered hits within genomes (<10kb between genes). Across the 10 *Variovorax*  
726 isolates scanned, we could not reconstruct any hotspot that recapitulated the previously described  
727 operon. Additionally to the *iac* operon, we scanned the auxin degradation operon described in  
728 (51) and could not identify it across the *Variovorax* isolates. Another piece of evidence that  
729 supports the fact that *Variovorax* lack these degradation operons was the weak (< 30%) identity  
730 between the spurious hits we did find to some of the components of these operons across the  
731 *Variovorax* genomes.

732 We searched for the ACC deaminase gene by looking for the KEGG orthology id K01505 (1-  
733 aminocyclopropane-1-carboxylate deaminase) across our genomes.

734

735 **References and Notes:**

- 736 1. K. Hiruma *et al.*, Root Endophyte *Colletotrichum tofieldiae* Confers Plant Fitness Benefits  
737 that Are Phosphate Status Dependent. *Cell*. **165**, 464–474 (2016).
- 738 2. G. Castrillo *et al.*, Root microbiota drive direct integration of phosphate stress and  
739 immunity. *Nature*. **543** (2017), doi:10.1038/nature21417.
- 740 3. P. Durán *et al.*, Microbial Interkingdom Interactions in Roots Promote *Arabidopsis* Survival.  
741 *Cell*. **175**, 973–983.e14 (2018).
- 742 4. S. Herrera Paredes *et al.*, Design of synthetic bacterial communities for predictable plant  
743 phenotypes. *PLOS Biol.* **16**, e2003962 (2018).
- 744 5. A. C. Huang *et al.*, A specialized metabolic network selectively modulates *Arabidopsis* root  
745 microbiota. *Science* **364**, eaau6389 (2019).
- 746 6. S. A. Hogenhout, R. A. L. Van der Hoorn, R. Terauchi, S. Kamoun, Emerging Concepts in  
747 Effector Biology of Plant-Associated Organisms. *Mol. Plant-Microbe Interact.* **22**, 115–122  
748 (2009).
- 749 7. D. Faure, D. Vereecke, J. H. J. Leveau, Molecular communication in the rhizosphere. *Plant  
750 Soil*. **321**, 279–303 (2009).
- 751 8. P. Mylona, K. Pawlowski, T. Bisseling, Symbiotic Nitrogen Fixation. *Plant Cell*. **7**, 869–885  
752 (1995).
- 753 9. Y. Helman, L. Chernin, Silencing the mob: disrupting quorum sensing as a means to fight  
754 plant disease. *Mol. Plant Pathol.* **16**, 316–329 (2015).
- 755 10. J. H. J. Leveau, S. E. Lindow, Utilization of the plant hormone indole-3-acetic acid for  
756 growth by *Pseudomonas putida* strain 1290. *Appl. Environ. Microbiol.* **71**, 2365–71 (2005).
- 757 11. A. Zúñiga *et al.*, Quorum Sensing and Indole-3-Acetic Acid Degradation Play a Role in  
758 Colonization and Plant Growth Promotion of *Arabidopsis thaliana* by *Burkholderia  
759 phytofirmans* PsJN. *Mol. Plant-Microbe Interact.* **26**, 546–553 (2013).
- 760 12. J. R. Leadbetter, E. P. Greenberg, Metabolism of acyl-homoserine lactone quorum-sensing  
761 signals by *Variovorax paradoxus*. *J. Bacteriol.* **182**, 6921–6 (2000).
- 762 13. C. R. Fitzpatrick *et al.*, Assembly and ecological function of the root microbiome across  
763 angiosperm plant species. *Proc. Natl. Acad. Sci. U. S. A.* **115**, E1157–E1165 (2018).
- 764 14. A. V. Klepikova, A. S. Kasianov, E. S. Gerasimov, M. D. Logacheva, A. A. Penin, A high  
765 resolution map of the *Arabidopsis thaliana* developmental transcriptome based on RNA-  
766 seq profiling. *Plant J.* **88**, 1058–1070 (2016).
- 767 15. N. Uchida *et al.*, Chemical hijacking of auxin signaling with an engineered auxin–TIR1 pair.  
768 *Nat. Chem. Biol.* **14**, 299–305 (2018).
- 769 16. T. Takase *et al.*, *ydk1-D*, an auxin-responsive *GH3* mutant that is involved in hypocotyl  
770 and root elongation. *Plant J.* **37**, 471–483 (2004).
- 771 17. L. Chen, I. C. Dodd, J. C. Theobald, A. A. Belimov, W. J. Davies, , The rhizobacterium  
772 *Variovorax paradoxus* 5C-2, containing ACC deaminase, promotes growth and  
773 development of *Arabidopsis thaliana* via an ethylene-dependent pathway. *J. Exp. Bot.* **64**,  
774 1565–1573 (2013).
- 775 18. A. J. Cary, W. Liu, S. H. Howell, Cytokinin action is coupled to ethylene in its effects on the  
776 inhibition of root and hypocotyl elongation in *Arabidopsis thaliana* seedlings. *Plant Physiol.*

777 107, 1075–82 (1995).

778 19. L. Gómez-Gómez, G. Felix, T. Boller, A single locus determines sensitivity to bacterial  
779 flagellin in *Arabidopsis thaliana*. *Plant J.* **18**, 277–284 (1999).

780 20. P. Nagpal *et al.*, AXR2 encodes a member of the Aux/IAA protein family. *Plant Physiol.*  
781 **123**, 563–74 (2000).

782 21. A. E. Hall, J. L. Findell, G. E. Schaller, E. C. Sisler, A. B. Bleecker, Ethylene perception by  
783 the ERS1 protein in *Arabidopsis*. *Plant Physiol.* **123**, 1449–58 (2000).

784 22. B. W. Bardoel *et al.*, *Pseudomonas* Evades Immune Recognition of Flagellin in Both  
785 Mammals and Plants. *PLoS Pathog.* **7**, e1002206 (2011).

786 23. S. L. Sun, W. L. Yang, W. W. Fang, Y. X. Zhao, L. Guo, Y. J. Dai, The Plant Growth-  
787 Promoting *Rhizobacterium Variovorax boronicumulans* CGMCC 4969 Regulates the Level  
788 of Indole-3-Acetic Acid Synthesized from Indole-3-Acetonitrile. *App. Environ. Microbiol.* **84**,  
789 00298–18 (2018).

790 24. S. J. Gould, E. S. Vrba, Exaptation—a Missing Term in the Science of Form. *Paleobiology*.  
791 **8**, 4–15 (1982).

792 25. A. Levy *et al.*, Genomic features of bacterial adaptation to plants. *Nat. Genet.* **50**, 138–150  
793 (2018).

794 26. O. M. Finkel *et al.*, The effects of soil phosphorous content on microbiota are driven by the  
795 plant phosphate starvation response. *bioRxiv*, 608133 (2019).

796 27. D. S. Lundberg, S. Yourstone, P. Mieczkowski, C. D. Jones, J. L. Dangl, Practical  
797 innovations for high-throughput amplicon sequencing. *Nat. Methods* **10**, 999–1002 (2013).

798 28. S. M. Yourstone, D. S. Lundberg, J. L. Dangl, C. D. Jones, MT-Toolbox: improved amplicon  
799 sequencing using molecule tags. *BMC Bioinformatics* **15**, 284 (2014).

800 29. N. Joshi, J. Fass, Sickle: A sliding-window, adaptive, quality-based trimming tool for FastQ  
801 files (Version 1.33) [Software]. Available at <https://github.com/najoshi/sickle>. (2011).

802 30. R. C. Edgar, Search and clustering orders of magnitude faster than BLAST. *Bioinformatics*.  
803 **26**, 2460–2461 (2010).

804 31. R. C. Edgar, UPARSE: highly accurate OTU sequences from microbial amplicon reads.  
805 *Nat. Methods* **10**, 996–998 (2013).

806 32. Q. Wang, G. M. Garrity, J. M. Tiedje, J. R. Cole, Naive Bayesian Classifier for Rapid  
807 Assignment of rRNA Sequences into the New Bacterial Taxonomy. *Appl. Environ. Microbiol.* **73**,  
808 5261–5267 (2007).

809 33. T. Z. DeSantis *et al.*, Greengenes, a chimera-checked 16S rRNA gene database and  
810 workbench compatible with ARB. *Appl. Environ. Microbiol.* **72**, 5069–72 (2006).

811 34. J. Oksanen *et al.*, “Package ‘vegan’” (2015).

812 35. M. I. Love, W. Huber, S. Anders, Moderated estimation of fold change and dispersion for  
813 RNA-seq data with DESeq2. *Genome Biol.* **15**, 550 (2014).

814 36. J. Schindelin *et al.*, Fiji: an open-source platform for biological-image analysis. *Nat.*  
815 *Methods* **9**, 676–682 (2012).

816 37. Package “emmeans” Type Package Title Estimated Marginal Means, aka Least-Squares  
817 Means (2019), doi:10.1080/00031305.1980.10483031.

818 38. J. Logemann, J. Schell, L. Willmitzer, Improved method for the isolation of RNA from plant  
819 tissues. *Anal. Biochem.* **163**, 16–20 (1987).

820 39. undefined A. S. Babraham Bioinformatics - FastQC A Quality Control tool for High  
821 Throughput Sequence Data, 3–5 (2018).

822 40. A. M. Bolger, M. Lohse, B. Usadel, Trimmomatic: a flexible trimmer for Illumina sequence  
823 data. *Bioinformatics*. **30**, 2114–20 (2014).

824 41. D. Kim, B. Langmead, S. L. Salzberg, HISAT: a fast spliced aligner with low memory  
825 requirements. *Nat. Methods*. **12**, 357–60 (2015).

826 42. Y. Liao, G. K. Smyth, W. Shi, The Subread aligner: fast, accurate and scalable read  
827 mapping by seed-and-vote. *Nucleic Acids Res.* **41**, e108 (2013).

828 43. P. Ewels, M. Magnusson, S. Lundin, M. Käller, MultiQC: summarize analysis results for  
829 multiple tools and samples in a single report. *Bioinformatics*. **32**, 3047–3048 (2016).

830 44. T. J. Wheeler, S. R. Eddy, nhmm: DNA homology search with profile HMMs.  
831 *Bioinformatics*. **29**, 2487–2489 (2013).

832 45. K. Katoh, D. M. Standley, MAFFT multiple sequence alignment software version 7:  
833 improvements in performance and usability. *Mol. Biol. Evol.* **30**, 772–80 (2013).

834 46. S. Capella-Gutiérrez, J. M. Silla-Martínez, T. Gabaldón, trimAI: a tool for automated  
835 alignment trimming in large-scale phylogenetic analyses. *Bioinformatics*. **25**, 1972–3  
836 (2009).

837 47. M. N. Price, P. S. Dehal, A. P. Arkin, FastTree 2 – Approximately Maximum-Likelihood  
838 Trees for Large Alignments. *PLoS One*. **5**, e9490 (2010).

839 48. S. A. Gordon, R. P. Weber, Colorimetric estimation of ilidoleacetic acid, *Plant Physiol.* **26**,  
840 192–5 (1951).

841 49. J. Friml *et al.*, Efflux-dependent auxin gradients establish the apical–basal axis of  
842 Arabidopsis. *Nature*. **426**, 147–153 (2003).

843 50. R. Donoso, P. Leiva-Novoa, A. Zúñiga, T. Timmermann, G. Recabarren-Gajardo, B.  
844 González, *Appl. Environ. Microbiol.* 83, e01991-16 (2016).

845 51. C. Ebenau-Jehle, M. Thomas, G. Scharf, D. Kockelkorn, B. Knapp, K. Schühle, J. Heider,  
846 G. Fuchs, *J. Bacteriol.* **194**, 2894–903 (2012).

847

848

849 **Acknowledgments:** We thank Stratton Barth, Julia Shen, Ellie Wilson, May Priegel and Dilan  
850 Chudasma for technical assistance; Dale Pelletier, DOE-ORNL for strains; the Dangl lab  
851 microbiome group for useful discussions; Anna Stepanova, Jose Alonso, Javier Brumos (North  
852 Carolina State University, USA), Joseph Kieber, Jason Reed (UNC Chapel Hill), and Isaac  
853 Greenhut (University of California, Davis) for useful discussions and Derek Lundberg (Max  
854 Planck Institute for Developmental Biology, Tübingen, Germany), and Anthony Bishopp  
855 (University of Nottingham, UK) for critical comments on the manuscript. **Funding:** This work  
856 was supported by NSF INSPIRE grant IOS-1343020 and by Office of Science (BER), U.S.  
857 Department of Energy, Grant DE-SC0014395 to J.L.D. J.L.D is an Investigator of the Howard  
858 Hughes Medical Institute, supported by the HHMI. P.J.P.L.T was supported in part by the Pew  
859 Latin American Fellows Program in the Biomedical Sciences (grant number 00026198). O.M.F  
860 was supported by NIH NRSA Fellowship F32-GM117758.

861

862 **Competing interests:** J.L.D. is a co-founder of, and shareholder in, AgBiome LLC, a corporation  
863 whose goal is to use plant-associated microbes to improve plant productivity

864

865 **Data and materials availability:**

866 The 16S amplicon sequencing data associated with this study is deposited in the NCBI SRA  
867 archive under the project accession PRJNA543313. The raw transcriptomic data is deposited in  
868 the Gene Expression Omnibus (GEO) under the accession GSE131158. In addition to the  
869 supplementary tables, we deposited all scripts and additional data structures required to  
870 reproduce the results of this study in the following GitHub repository:  
871 <https://github.com/isa1sg/variivoraxRGI>